Multimedia Systems
DOI 10.1007/s00530-016-0526-5

REGULAR PAPER

Towards professionally user-adaptive large medical image transmission processing in mobile telemedicine systems

Yi Zhuang[1] · Nan Jiang[2] · Qing Li[3] · Hua Hu[4] · Dickson K. W. Chiu[5]

Received: 16 July 2015 / Accepted: 22 July 2016

Abstract To effectively and efficiently reduce the transmission costs of large medical image in (mobile) telemedicine systems, we design and implement a professionally user-adaptive large medical image transmission method called *UMIT*. Before transmission, a preprocessing step is first conducted to obtain the optimal image block (IB) replicas based on the users' professional preference model and the network bandwidth at a master node. After that, the candidate IBs are transmitted via slave nodes according to the transmission priorities. Finally, the IBs can be reconstructed and displayed at the users' devices. The proposed method includes three enabling techniques: (1) *user's preference degree derivation of the medically useful areas*, (2) *an optimal IB replica storage scheme*, and (3) *an adaptive and robust multi-resolution-based IB replica selection and transmission method*. The experimental results show that the performance of our proposed *UMIT* method is both efficient and effective, minimizing the response time by decreasing the network transmission cost.

Keywords Medical image · Multi-resolution · Mobile telemedicine system · Image replica · User-adaptive

1 Introduction

1.1 Motivations

Telemedicine is the use of medical information exchanged from one site to another via electronic communications to improve, maintain, or assist patients' health status [1]. Telemedicine system (*TS*) is a rapidly developing application of clinical medicine, where medical information (e.g., medical image) is transferred through the Internet and other networks for the purpose of remote medical procedures, consulting, and examinations. Compared with the traditional face-to-face interaction of patients and physicians, with the aid of the *TS*, patient diagnosis in the remote (rural) areas can be conducted conveniently with lower costs. With recent advances in mobile network and medical technologies, mobile telemedicine systems (*MTS*) have emerged to deal with medical diagnosis, treatment, health monitoring, etc. Compared with the traditional *TS*s, *MTS*s have three main characteristics: (1) Mobility of users: most users using *MTS* are constantly moving, which means the spatial position of each user varies with time; (2) Lower processing capability: the processing and battery capacities of the most mobile client devices (e.g., cell phone, PDA, etc.) are limited, which motivates us to devise a energy-efficient technique to support image transmission with optimized costs; (3) Instability and heterogeneity of mobile networks (*MN*): *MN* for *MTS* is often instable that means some nodes

Communicated by B. Prabhakaran.

✉ Yi Zhuang
zy158cn@gmail.com

[1] College of Computer and Information Engineering, Zhejiang Gongshang University, Hangzhou, People's Republic of China

[2] Hangzhou First People's Hospital, Hangzhou, People's Republic of China

[3] Department of Computer Science, City University of Hong Kong, Hong Kong, People's Republic of China

[4] School of Computer, Hangzhou Dianzi University, Hangzhou, People's Republic of China

[5] Faculty of Education, The University of Hong Kong, Hong Kong, People's Republic of China

Published online: 20 August 2016

may be down or connected intermittently to the network, and the bandwidth between any two nodes may vary with time.

Patents' medical images are a key basis to facilitate diagnosis. For the transmission and browsing of large medical images in *TS*s, network transmission cost of such images accounts for a large percentage of the overall interaction time [2]. Therefore, the reduction of transmission cost, especially in the *MTS*s, is very critical to the overall performance improvement. To achieve this, a scalable, high-throughput, location-based transmission scheme is generally required [3]. For physicians in different departments, however, they have different professional preferences[1] to the medical images that include different lesion organs, corresponding to regions in the images called medically useful area (MUA)s. For example, for a medical image, including two lesion organs (e.g., lung and liver), in most cases, it is natural for a physician from the respiration department to pay much attention to the lung than the liver and the rest of the image called non-MUA. Therefore, to effectively reduce the total transmission cost, the pixel resolutions of the MUAs and the non-MUA can be moderately adjusted, provided that will not affect the image examination. In this case, the pixel resolution of the MUA replica of the liver organ can be relatively lower than that of the lung and the non-MUA. Thus, the total image data size can be effectively reduced to optimize the total transmission cost accordingly. In addition, as different receivers (i.e., physician) have different users' preference degree (UPD)s for the different MUAs in an image, the MUAs that have higher UPDs can be transmitted with higher pixel resolutions and transmission priorities. Although considerable amount of research efforts has been carried out on image transmission [4–7], most of them focused on two ways without considering the special requirements of medical applications as mentioned above: (1) improvement of the data transmission protocol [4–7, 10, 18]; and (2) content-based image data compression [8, 9, 11–17]. The data transmission efficiencies of these two approaches are limited, because the response time is linearly increasing with the size of the transferred file. To the best of our knowledge, a little research has been touched on the medical image transmission performance improvement from both of the two perspectives: the image content and user's professional preferences.

To address these aspects, we devise a user-adaptive medical image transmission (*UMIT*) scheme that not only considers the image content and the network bandwidth, but also the physicians' professional preferences. In particular, exploring the users' professional preferences to speed up the transmission processing and improve user experiences is a new research direction, which has received a little attention so far.

[1] Strictly speaking, the professional preference refers to the organ(s) that a physician is specialized (or interested) in.

1.2 Technical challenges

The technical challenges of designing our high-performance personalized medical image transmission method include the four main aspects:

1. Applying professional preference model to medical image transmission: a medical image is composed of some salient objects (i.e., MUA) with UPDs varying for different users, and their transmission pixel resolutions are proportional to their UPDs. The question is how to establish a relationship between MUAs and users' preferences?
2. High computation cost in medical image transmission: most of medical images are characterized by high pixel resolution, high dimensional, and large scale. Therefore, the computation and transmission costs of such medical images are very high.
3. Mobility of *MN* users: as most users in the *MN* are constantly moving, which means the spatial position of each user varies with time. Therefore, how to perform an optimal data placement is also a challenging issue.
4. Instability and heterogeneity of the *MN*: the nodes in the *MN* are instable that means some nodes may be down or connected intermittently in the network. The bandwidth between any two nodes in the *MN* may vary with time. There is no guarantee that the total response time of each transmission will be similar.

1.3 Contributions

To address the above challenges, we have implemented the *UMIT* method and the contributions of this paper can be summarized as follows:

- We introduce a framework of a user-adaptive medical image transmission scheme in mobile telemedicine systems (*UMIT*).
- We propose a user's professional preference model to support *UMIT* processing.
- We present three enabling techniques, namely, *UPDs derivation of the MUAs*, *optimal IB replica storage scheme*, and *adaptive and robust transmission scheme* to progressively reduce the communication cost in the *MN* environment and improve users' experiences.
- We conduct extensive experimental studies to evaluate the effectiveness, efficiency, scalability, and robustness of our proposed method for medical image transmission.

The remainder of the paper is organized as follows. Section 2 reviews related works and Sect. 3 presents preliminary definitions and system overview. In Sect. 4, we introduce a user's professional preference model. Three enabling techniques are presented to facilitate the user-adaptive medical image transmission processing in Sect. 5. After that, we propose an image transmission scheme called the *UMIT* in Sect. 6. In Sect. 7, we perform comprehensive experiments to evaluate the efficiency of our proposed approach before we conclude the paper in the final section.

2 Related work

Image data transmission techniques have been extensively studied for about 20 years [4–9]. The state-of-the-art methods can be mainly divided into two categories: (1) improvement of transmission protocol [4–6, 9, 10, 18]; and (2) image data encoding and compression [8–17].

Charles et al. [4] first presented a wireless image data transmission method from end to end, and provided some experimental analysis. John et al. [5] proposed a fast lossy Internet image transmission scheme for images which eliminates retransmission delays by strategically shielding important portions of the image with redundancy bits. After that, Raman et al. [6] proposed an image transmission protocol called ITP. Comparing with the traditional TCP protocol, the ITP is more suitable for image data transmission. Packet losses just decrease the quality of image or video in multimedia applications. Robustness to packet losses is crucial to high-quality image transmission in Internet or wireless channels, where data loss often happens. Based on compressive sensing, Gao et al. [10] proposed a robust image transmission scheme for wireless channels. Since high packet error rates and the need for retransmission make it inefficient in terms of energy and bandwidth, recently, Aziz et al. [18] have designed a novel architecture and protocol for energy-efficient image processing and communication over wireless sensor networks.

Chang et al. [11] presented a progressive image transmission (PIT) scheme, which transmits the most significant portion of a picture, followed by less important parts. Lin et al. [8] presented a compound image compression algorithm for real-time applications of computer screen image transmission called shape primitive extraction and coding (SPEC). Ruiz et al. [9] designed an image compression algorithm to support progressive image transmission. Available PIT mechanisms and systems can be categorized into spatial domain [12] and pyramid-structured progressive transmission [15]. A progressive image transmission in the spatial domain is called the bit plane method (BPM) [14, 16], in which the final transmitted image is the same as the original. However, its high transmission bit rate is a major disadvantage. Due to the drawback of BPM, lossy PIT techniques have received more attention. To provide a fast PIT scheme, Chang et al. [13] improved the BPM method called the guessing by neighbors (GBN), in which fifty percent of the pixels are transmitted, while the other fifty percent were "guessed". Based on the Reed–Solomon coding, Pinar et al. [17] designed a robust image transmission over wireless sensor networks. Sun et al. [19] proposed a progressive image transmission system over wireless channels by combining joint source–channel coding (JSCC), space–time coding, and orthogonal frequency division multiplexing (OFDM). Victor et al. [20] devised a 3D scalable medical image compression method with optimized volume of interest coding. Recently, Arslan et al. [21] have proposed a generalized unequal error protection LT codes for progressive data transmission.

Besides image transmission, Hoppe [23] introduced a new progressive mesh (PM) scheme for storing and transmitting arbitrary triangle meshes. Teler and Lischinski [24] proposed a streaming method of complex 3D scenes for remote walkthroughs. Rusinkiewicz and Levoy [25] designed a viewer for networked visualization of large, dense models. Gu et al. [26] proposed to remesh an arbitrary surface onto a completely regular structure called geometry image. Bischoff and Kobbelt [27] proposed a robust approach for broadcasting of geometric data. Lamberti and Sanna [28] introduced a streaming-based solution for remote visualization of 3D graphics on mobile devices. Cheng et al. [29] proposed an analytical model for progressive mesh streaming. Kumar1 and Mishra [30] presented a 3D object transmission scheme over the Internet using 2D image streaming technology.

In our previous work [22], we have proposed a content-aware and multi-resolution-based medical image transmission scheme, in which only two factors, image content and network bandwidth, are considered for optimizing the transmission. Different from the above state-of-the-art methods, this paper proposes a user-adaptive medical image data transmission method, in which the three factors, i.e., the receiver users' professional preferences, the image content, and network bandwidth, are holistically analyzed to obtain optimized transmission pixel resolution for different IBs. To the best of our knowledge, this is the first work to improve the transmission performance from the perspectives of the user's professional preferences on image contents.

3 Preliminaries and system overview

The list of symbols to be used throughout the rest of this paper is summarized in Table 1.

Table 1 List of notations

Symbol	Description
Ω	A set of medical images
$\Omega(j)$	The medical images in the jth local slave node
I_S	A transmission medical image and $I_S \in \Omega$
MUA_i	The ith MUA in a medical image and $i \in [1, \lvert\text{MUA}\rvert]$
R	The rest of the image I_S (i.e., non-MUA)
IF	Image fragment (i.e., MUA and R)
IB	Image block
dpi	Dots per inch
D_L, D_U	The lower and upper bounds of the dpi, respectively
E_L, E_U	The lower and upper bounds of the network bandwidth, respectively
$UPPV$	User professional preference vector
PUS	Pivot user set
UPD	User preference degree
m	The number of organs(or professional preferences)
$\lvert\text{MUA}\rvert$	The number of MUAs in an image
h	The number of pivot users
U_R	A receiver user
U_P^j	The jth pivot user and $j \in [1, h]$
Δ	Granularity value both for network bandwidth and the image pixel resolution

Definition 1 A mobile network (*MN*) is a graph that is modeled by a triplet:

$$MN := \langle N, E, T \rangle \tag{1}$$

where N refers to the set of nodes and E refers to a set of edges representing the network bandwidths for data transmission at time T.

As the data and message communication in an *MTS* is based on an *MN* environment, due to the instability and heterogeneity of the *MN* environment, the bandwidth of any two nodes in *MN* may be different and varies with time. In addition, the data transmission distance in an *MN* is limited.

Definition 2 The nodes in *MN* can be logically divided into three categories: master nodes (N_M), slave nodes (N_S), and receiver nodes (N_R), formally denoted as $N = N_M \cup N_S \cup N_R$, where

- N_M is responsible for: (1) transmission request routing, and (2) collecting and analyzing the network bandwidth and receivers' information for optimal transmission pixel resolutions of IB replicas;
- N_S is responsible for: (1) storing the IB replicas with different pixel resolutions and transmission priorities, and (2) sending the replicas to the receivers; and
- N_R is responsible for receiving and reconstructing the IB replicas at the receiver devices.

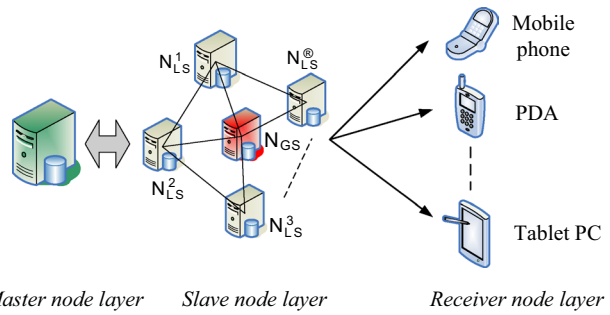

Fig. 1 Three-layer architecture in a *TS*

As shown in Fig. 1, for the slave nodes in the *MN*, they can be further divided into two types: global slave nodes (N_{GS}) and local slave nodes (N_{LS}).

Definition 3 (*Global Slave Node*) A global slave node, denoted as N_{GS}, is a slave node for storing the partial IB replicas that are not frequently accessed.

Definition 4 (*Local Slave Node*) A local slave node, denoted as N_{LS}, is another type of slave node to store the partial IB replicas that are frequently accessed, N_{LS} is

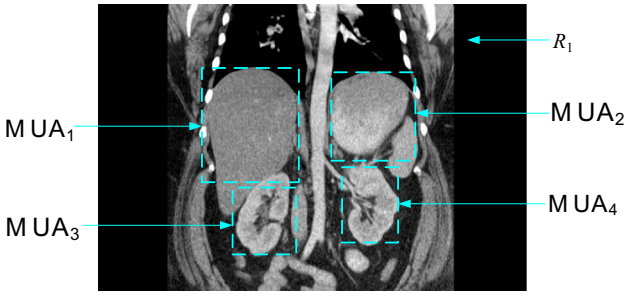

Fig. 2 Four MUAs in a medical image

composed of α slave nodes (N^i_{LS}), where N^i_{LS} is the ith N_{LS}, for $i \in [1, \alpha]$.

For each image, in most cases, there exist some salient objects that users are interested in. The regions of such salient objects are called *medically useful area* (MUA)s.

Definition 5 A medically useful area (MUA) in an image can be modeled by a six-tuple:

$$\mathrm{MUA}_i := \langle i,\ O,\ S,\ pos,\ dpi,\ pr \rangle \tag{2}$$

where i is the ID number of the MUA, O represents the organ that the MUA corresponds to, S is the area value of the MUA, *pos* is the coordinate position of the MUA in the image, *dpi* refers to the dots per inch for the MUA, and *pr* is the probability that a user is interested in the MUA.

Definition 6 The rest part of an image (R) can be modeled by a two-tuple:

$$R := \langle S,\ dpi \rangle \tag{3}$$

where S is the area value of the R and *dpi* refers to the dots per inch for the R.

Based on Definitions 5 and 6, in Fig. 2, there exist four MUAs (MUA$_1$, MUA$_2$, MUA$_3$, and MUA$_4$), and one $R(R_1)$ in the image, in which the corresponding MUA areas are preliminarily identified by the discriminately trained deformable part model-based approach [32]. Each MUA corresponds to an organ. For example, MUA$_1$.O = "*liver*", MUA$_2$.O = "*spleen*", MUA$_3$.O = "*kidney*", and MUA$_4$.O = "*kidney*". The probabilities that the receiver is interested in the MUAs of the image are defined by their corresponding UPDs.

Definition 7 (*User Preference Degree*) Given an MUA_i in an image and a user U_j, its corresponding user's preference degree (UPD) is the probability that U_j is interested in MUA$_i$, denoted as: UPD$(MUA_i, U_j) \in [0, 1]$, where $i \in [1, |MUA|]$.

As mentioned before, for a medical image, it can be equally partitioned into image blocks.

Definition 8 (*Image Block*) Given an image block IB_i, it can be modeled by a five-tuple:

$$IB_i := \langle i, S, pos, TP, dpi \rangle \tag{4}$$

where i refers to the ID number of the IB, S is the area value of the IB, *pos* is the coordinate position of the IB in the image, *TP* refers to the transmission priority of the IB and $TP \in [0, 1]$, and *dpi* means the corresponding pixel resolution of the IB.

Figure 3 shows the data flow diagram of *UMIT* processing. The basic idea behind the transmission scheme is that given a medical image I_S, the pixel resolutions of its MUAs that are equal to the user's preference organs with high UPDs are kept high, and different UPDs correspond to different pixel resolutions of the MUAs. The resolution of the rest of the image can be reduced according to other factors, such as network bandwidth, its corresponding area, etc. Concretely, first of all, in the preprocessing step of the *UMIT*, for each image I_i, its corresponding MUAs are first logically identified and drew manually by users. Then, the image is physically and equally partitioned into some blocks, denoted as IB, the IBs in MUAs, and the rest part are placed at the slave nodes with different pixel resolutions and transmission priorities. As the MUAs are the main contents of the image, they are critically important to the *UMIT* processing, in which their original pixel resolutions can only be adjusted moderately based on the different

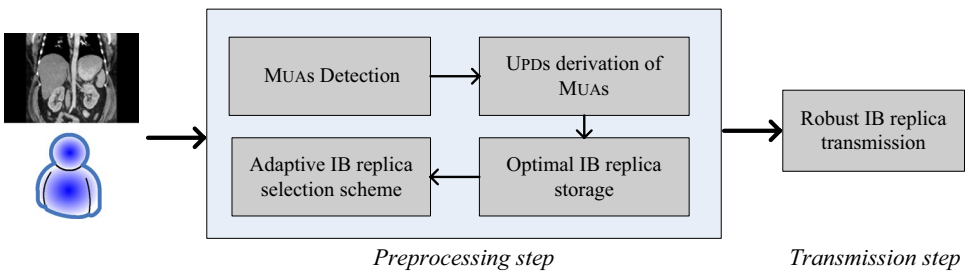

Fig. 3 Data flow chart of the *UMIT* processing

Table 2 Example of the UPPV for U_i

PO	*Brain*	*Lung*	*Heart*	*Liver*	*Kidney*	…	*Intestine*
Pr	0	30 %	20 %	60 %	10 %	…	0

UPDs. For the rest of the image, both of its pixel resolution and transmission priority are lower than that of the MUAs, so that the main part of the image can be transmitted and displayed in priority. Once the preprocessing step is completed, the next step is to perform the *UMIT* processing. Specifically, when a medical image I_S is prepared to transmit, the information, such as user's professional preferences, current network bandwidth, and receivers' identity needs to be collected and analyzed uniformly to derive the optimal pixel resolutions of the IB replicas for the different MUAs and the rest part in I_S. Then, the candidate IBs are transmitted to the receiver node (N_R) from the slave ones (N_S) based on their transmission priorities. Finally, the IBs are reconstructed and displayed at the receiver nodes.

The goal of our proposed method is to transmit a large medical image adaptively in the *MTS*s with minimal data communication and CPU costs based on users' professional preferences.

4 Modeling user's professional preference

As the first step in the transmission preprocessing step, it is critically important to model user's professional preferences. The basic idea is that for a receiver U_R, his user's preferences can be first initialized and derived from his nearest neighbor pivot users based on their user similarity distance (*USD*). Therefore, in this section, we first give a definition of the user's professional preference vector (*UPPV*) in Sect. 4.1. Then, in Sect. 4.2, three approaches are developed to construct the *UPPV*s of the pivot users. Finally, we propose a user's preference propagation method to in Sect. 4.3.

4.1 User's professional preference vector

As mentioned before, for each user U_i, the corresponding preference distributions with probabilistic guarantees are important to facilitate user-adaptive medical image transmission processing. Therefore, as a preprocessing step, it is critical to build a user's preference vector for each receiver, which is defined as follows.

Definition 9 (*User Professional Preference Vector, UPPV*) The user's professional preference vector of a user U_i, denoted as $UPPV_i$, is a vector represented as:

$$UPPV_i = \langle (PO_1, Pr_1), (PO_2, Pr_2), \ldots, (PO_m, Pr_m) \rangle \tag{5}$$

where i refers to the user ID, PO_j is the jth professional organ(preference), and Pr_j is the probability that the user is interested in PO_j.

Note that, for easy illustration, the professional organ refers to a lesion organ of a disease, a physician specializes in. Table 2 shows an example of the *UPPV* of U_i, in which the probabilities that U_i likes different *PO*s are illustrated.

4.2 *UPPV*s construction for pivot users

Before introducing the *UPPV*s construction, the MUAs in the n images of Ω have been identified and the corresponding organs in the MUAs have been annotated (e.g., "*lung*" "*heart*" etc). For a pivot user, the corresponding *UPPV* can be constructed by three approaches, namely, implicit, explicit, and unified.

- *Implicit approach*

- The *UPPV* model can be implicitly established as follows: given a pivot user U_P^j and the n medical images $I_i \in \Omega$, we first count the times of the corresponding organs in the MUA accessed in each of the n medical images. Then, the probability that U_P^j is interested in the kth preference organ can be derived as:

$$Pr_k = \frac{\sum\limits_{\substack{t \in [1, |I_i.MUA|] \\ i \in [1,n], k \in [1,m]}} 1_{\{MUA_t.O = PO_k\}}}{\sum_{i=1}^{n} |I_i.MUA|} \tag{6}$$

Finally, we can obtain the *UPPV* which is represented as a vector in the following:

$$UPPV_1(U_P^j) = \{\langle PO_1, Pr_1 \rangle, \langle PO_2, Pr_2 \rangle, \ldots, \langle PO_m, Pr_m \rangle\} \tag{7}$$

where PO_k is the kth preference organ, Pr_k is the probability that U_P^j is interested in PO_k in Eq. (7), and $k \in [1,m]$.

- *Explicit approach* Next, we study an explicit approach to build the *UPPV* model by using a user's preference profile. For the user's professional preference distribution, it can be represented by a vector:

$$UPPV_2(U_P^j) = \{\langle PO_1, pr_1\rangle, \langle PO_2, pr_2\rangle, \ldots, \langle PO_m, pr_m\rangle\} \tag{8}$$

where pr_k is the probability that user prefers to PO_k.

- *Unified approach* Finally, based on the above two approaches, we propose a unified approach to obtain the *UPPV* model by merging the above two vectors, which is uniformly derived in the following:

$$UPPV(U_P^j) = \left\{\left\langle PO_1, \frac{Pr_1 + pr_1}{2}\right\rangle, \left\langle PO_2, \frac{Pr_2 + pr_2}{2}\right\rangle, \ldots, \left\langle PO_m, \frac{Pr_m + pr_m}{2}\right\rangle\right\} \tag{9}$$

4.3 User's professional preference propagation

As mentioned above, for user-adaptive transmission processing, it is important to obtain the user's professional preference profile information in advance, but we cannot expect users enter them manually. Therefore, in this subsection, we propose a pivot-based user's professional preference propagation method.

4.3.1 User similarity distance

Definition 10 A physician can be modeled by a five-tuple:

$$U_i := \langle i, dep, pos, T, PO\rangle \tag{10}$$

where i denotes the user ID; T refers to the time; dep refers to the department that U_i is affiliated with, *pos* is the location coordinate value of U_i who submits image transmission at time T (denoted as *pos*:= <*lon*, *lat*>, where *lon* and *lat* refer to the longitude and latitude values, respectively); and *PO* means the preference organs that U_i is interested in.

Definition 11 Given two users: U_i and U_j, their user similarity distance (*USD*) can be derived as follows:

$$USD(U_i, U_j) = 1 - \frac{1}{2}\left(\sum_{\{U_i.\text{dep}=U_j.\text{dep}\}} 1 + \frac{|PO(U_i) \cap PO(U_j)|}{|PO(U_i) \cup PO(U_j)|}\right) \tag{11}$$

where $U_i.\ dep = U_j.\ dep$ means U_i and U_j are in a same department. $PO(U_i)$ means the preference organs that U_i prefers to and the probabilities that U_i are interested in these organs are larger than zero.

Based on Definition 11, smaller the *USD* is, closer (more similar) the two users are.

4.3.2 Learning from user's preferences

For user U_R, there are two scenarios in terms of the relationship between U_R and the pivot users. The first scenario is that U_R is from the pivot user set (*PUS*); and the second one is that U_R is not from the *PUS*.

- U_R from *PUS*

In the first scenario, the preference profile of the receiver user (U_R) can be easily obtained by matching the user name.

- U_R not from *PUS*

In the second scenario, as U_R is not from the *PUS*, it is not trivial to infer the corresponding professional preferences due to data sparsity. So, here, we explain how to derive

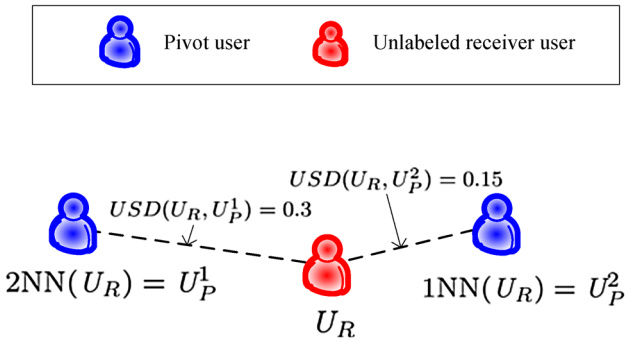

Fig. 4 *PL*-based derivation of the *UPPV*

Fig. 5 Example of the probability propagation

PO	*Prob.*
brain	75%
lung	8%
liver	5%
kidney	10%
intestine	2%

(a) Professional preference probability distribution of U_P^2

PO	*Prob.*
brain	63%
lung	4%
liver	3%
kidney	25%
intestine	5%

(b) Professional preference probability distribution of U_P^1

PO	*Prob.*
brain	71%
lung	6.7%
liver	4.3%
kidney	15%
intestine	3%

(c) Professional preference probability distribution of U_R

user's preferences through the propagation of that from the pivot ones. To address this problem, we first obtain an initial preference vector via learning the corresponding neighboring pivot ones with *UPPV*s already obtained.

The motivations of this method are based on the two observations: (1) physicians in a same department have similar professional preferences; (2) beside the organ, a physician is specialized or interested in, attention is often paid to nearby organs. Therefore, to obtain the *UPPV* of each receiver user, we first propose a pivot-learning(*PL*)-based derivation method, in which h users are randomly chosen as pivot ones. As mentioned above, the corresponding h *UPPV*s of these pivot users are obtained previously in Sect. 4.2. The aim of this method is to derive a *UPPV* of a user U_R via nearest neighbor pivot ones in terms of their *USD*s.

Specifically, let U_R be the receiver user, PO_j be the jth professional preference of U_R, and 1NN(U_R) and 2NN(U_R) be the two nearest neighbor pivot users of U_R. Then, the probability that the jth professional preference of U_R is Y can be approximately derived in Eq. (12) based on an intuition: the more similar the two users are, the higher the probability that their two corresponding professional preferences are equal.

$$\frac{\Pr(\text{2NN}(U_R) \text{ is interested in } PO_j) - \Pr(U_R \text{ is interested in } PO_j)}{\Pr(U_R \text{ is interested in } PO_j) - \Pr(\text{1NN}(U_R) \text{ is interested in } PO_j)} = \frac{USD(U_R, \text{2NN}(U_R))}{USD(U_R, \text{1NN}(U_R))} \tag{12}$$

Solving Eq. (12), the probability that U_R is interested in the professional preference (PO_j) can be represented in the following:

$$\begin{aligned}&\Pr(U_R \text{ is intersted in } PO_j)\\ &= \frac{\Pr(\text{2NN}(U_R) \text{ is interested in } PO_j) + \frac{USD(U_R, \text{2NN}(U_R))}{USD(U_R, \text{1NN}(U_R))} \cdot \Pr(\text{1NN}(U_R) \text{ is interested in } PO_j)}{\frac{USD(U_R, \text{2NN}(U_R))}{USD(U_R, \text{1NN}(U_R))} + 1}\\ &= \frac{USD(U_R, \text{1NN}(U_R)) . \Pr(\text{2NN}(U_R) \text{ is interested in } PO_j) + USD(U_R, \text{2NN}(U_R)) \cdot \Pr(\text{1NN}(U_R) \text{ is interested in } PO_j)}{USD(U_R, \text{2NN}(U_R)) + USD(U_R, \text{1NN}(U_R))}\end{aligned} \tag{13}$$

where PO_j can be professional preference organ, such as '*heart*', '*liver*', '*lung*', etc.

For example, suppose, there are three users (U_R, U_P^1, and U_P^2) in Fig. 4. The preference distributions of the two pivot users are shown in Fig. 5a and b. For user U_R, assume that $USD(U_R,U_P^1) = 0.3$, and $USD(U_R,U_P^2) = 0.15$. Therefore, we have $1\text{NN}(U_R) = U_P^2$ and $2\text{NN}(U_R) = U_P^1$. Based on Eq. (13), the probability that the U_R is interested in '*liver*' can be derived as follows:

$$
\begin{aligned}
&\Pr(U_R \text{ is interested in '}liver\text{'}) \\
&= \frac{USD(U_R,,1\text{NN}(U_i))\cdot \Pr(2NN(U_R)\ U_R \text{ is interested in '}liver\text{'}) + USD(U_R,,2\text{NN}(U_R))\cdot \Pr(1\text{NN}(U_R) \text{ is interested in '}liver\text{'})}{USD(U_R,,2\text{NN}(U_R)) + USD(U_R,,1\text{NN}(U_R))} \\
&= \frac{0.15\cdot \Pr(2\text{NN}(U_R) \text{ is interested in '}liver\text{'}) + 0.3\cdot \Pr(1\text{NN}(U_i) \text{ is interested in '}liver\text{'})}{0.3+0.15} \\
&= \frac{0.15\Pr\left(U_P^1 \text{ is interested in '}liver\text{'}\right) + 0.3\cdot \Pr\left(U_P^2 \text{ is interested in '}liver\text{'}\right)}{0.3+0.15} \\
&= \frac{0.15\cdot 0.03 + 0.3\cdot 0.05}{0.3+0.15} \\
&= 0.043
\end{aligned}
$$

Similarly, the probabilities that the user U_R is interested in '*brain*', '*lung*', '*kidney*', and '*intestine*' can be computed accordingly, as shown in Fig. 5c.

Algorithm 1 summarizes the *PL*-based *UPPV* construction algorithm.

Algorithm 1. The PL-based *UPPV* construction algorithm

Input: h pivot users U_P^j,
Output: the *UPPV* of U_R
1. $UPPV \leftarrow \Phi$; // *initialization*
2. find the two nearest neighbor pivot users to U_R, denoted as $1\text{NN}(U_R)$ and $2\text{NN}(U_R)$;
3. **for** each professional preference(PO_j) **do**
4. the probability that U_R is interested in PO_j is derived by Eq.(13);
5. add the probability and PO_j to the *UPPV*;
6. **end for**
7. **return** *UPPV*;

5 Enabling techniques

To better facilitate the user-adaptive medical image transmission processing, in this section, we introduce three enabling techniques: (1) *UPDs derivation of MUAs*, (2) *optimal IB replica storage scheme*, and (3) *adaptive and robust IB replica selection and transmission scheme*.

5.1 Deriving UPDs of MUAs

As analyzed in Sect. 4, we have obtained the user's professional preferences of U_R. To facilitate *UMIT* processing, the corresponding preference probabilities of different MUAs in I_S submitted by U_R need to be first derived via the *UPPV* model. Therefore, in this subsection, we study how to derive the UPDs of the MUAs in I_S.

First of all, in the preprocessing step, for a medical image I_S, its corresponding MUAs are first preliminarily identified using the discriminately trained deformable part model-based approach [32], in which some related organ names have been labeled manually. To support an efficient user-adaptive image transmission with high quality, the pixel resolution of each MUA can be adjusted based on the three factors, such as its corresponding UPD, the area of the MUA, and the network bandwidth, while the pixel resolution of the non-MUA part of the image can be reduced based on the network bandwidth and its area value.

Next, we study how to obtain the UPDs of all MUAs in a transmission image I_S based on our user's professional preference model. More specifically, in Fig. 6, assume that the preference organs of user U_R are PO_1, PO_2,..., and PO_m respectively, and the MUAs in I_S can be represented as: MUA_1, MUA_2,..., and $\text{MUA}_{|\text{MUA}|}$. First, for each MUA_j in I_S, find its corresponding PO_i in the *UPPV* with organ name equal to that of the MUA_j and its corresponding preference probability non-zero, then the UPD of MUA_j is the probability value (i.e., $PO_i.Pr$); otherwise, if the probability value is zero (i.e., $PO_i.Pr = 0$), we propose a distance-based probability propagation method to derive it, in which a body organ graph (*BOG*) (see Fig. 7) is introduced to calculate the distance between any two organs. Specifically, first of all, for the *UPPV* of user U_R, the organ with maximal probability in the vector is identified as a preference one (*PO*). Then, find its nearest neighbor organ in the *BOG*, denoted as NN(*PO*), with non-zero corresponding preference probability in the *UPPV*. For U_R, suppose an organ (O) has zero probability of the professional preference in his *UPPV*, to derive its UPD of its corresponding MUA, Eq. (14) holds:

$$
\frac{\Pr(U_R \text{ is interested in } PO) - \Pr(U_R \text{ is interested in } O)}{\Pr(U_R \text{ is interested in } PO) - \Pr(U_R \text{ is interested in NN}(PO))} = \frac{dist(\text{MUA}_1, \text{MUA}_2)}{dist(\text{MUA}_1, \text{MUA}_3)} \tag{14}
$$

where $dist(\text{MUA}_i, \text{MUA}_j)$ is the L_2 distance of the two corresponding organs of the two MUAs in the *BOG* and $dist\left(\text{MUA}_i, \text{MUA}_j\right) = \sqrt{\left(\text{MUA}_i.pos.x - \text{MUA}_j.pos.x\right)^2 + \left(\text{MUA}_i.pos.y - \text{MUA}_j.pos.y\right)^2}$.

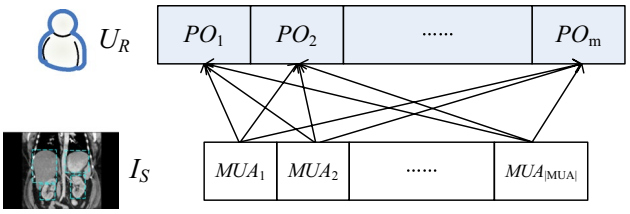

Fig. 6 UPD Derivation of the MUAs

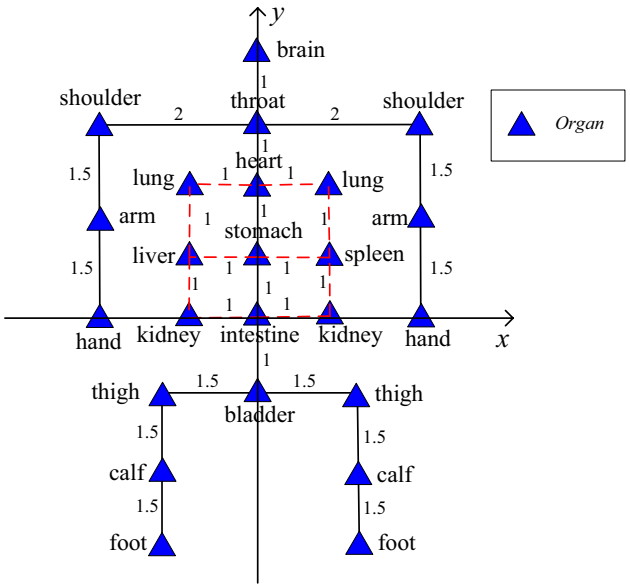

Fig. 7 Body organ graph

Solving Eq. (14), the probability that U_R is interested in the organ O is represented in the following:

$$\begin{aligned}&\Pr(U_R \text{ is interested in } O)\\&= \Pr(U_R \text{ is interested in } PO)\\&\quad - \frac{dist(\text{MUA}_1, \text{MUA}_2)}{dist(\text{MUA}_1, \text{MUA}_3)} \cdot (\Pr(U_R \text{ is interested in } PO))\\&\quad - \Pr(U_R \text{ is interested in } NN(PO)) \qquad (15)\end{aligned}$$

For example, assume that the *UPPV* of U_R is represented in Table 3. For a transmission image I_S, assume that there are three MUAs which are shown in Table 4.

In Fig. 7, since coordinates of the above three MUAs are: $\text{MUA}_1.pos = (-1, 1)$, $\text{MUA}_2.pos = (-1, 2)$, and $\text{MUA}_3.pos = (-1, 0)$, the distances between MUA_1 and MUA_2, and MUA_1 and MUA_3 are $dist(\text{MUA}_1, \text{MUA}_2) = 1$, and $dist(\text{MUA}_1, \text{MUA}_3) = 1$, respectively. As shown in Table 3, for U_R, as the probability that he is interested in "*lung*" is zero, based on Eq. (15), the probability that U_R is interested in MUA_2 (i.e., '*lung*') can be calculated below:

Table 3 Example of the UPPV of U_R

PO	*Brain*	*Lung*	*Liver*	*Kidney*	*Intestine*
Prob.	0 %	0 %	63 %	26 %	11 %

Table 4 Example of the four MUAs in I_S

MUA	MUA_1	MUA_2	MUA_3
Organ	*Liver*	*Lung*	*Kidney*

Table 5 Example of the user attention degrees of the three MUAs in I_S

MUA	MUA_1	MUA_2	MUA_3
Organ	Liver	Lung	Kidney
UPD	63 %	26 %	26 %
Normalized UPD	44.8 %	18.4 %	18.4 %

$$\begin{aligned}&\Pr(U_R \text{ is interested in '}lung\text{'})\\&= \Pr(U_R \text{ is interested in '}liver\text{'})\\&\quad - \frac{dist(\text{MUA}_1, \text{MUA}_2)}{dist(\text{MUA}_1, MUA_3)} \cdot (\Pr(U_R \text{ is interested in '}liver\text{'}))\\&\quad - \Pr(U_R \text{is interested in '}kidney\text{'})\\&= 0.63 - \frac{1}{1} \cdot (0.63 - 0.26)\\&= 0.26\end{aligned}$$

Therefore, the probability that U_R is interested in 'lung' is 26 %, shown as the UPD of the MUA_2 in Table 5. Furthermore, since the sum of the UPDs may be larger than 100 %, normalization is performed, so that the sum of the normalized UPDs is 100 %.

Algorithm 2 details how to obtain the UPDs of all MUAs via the content of the user preference organs.

Algorithm 2. ***Obtaining the UPDs of MUAs()***

Input: the MUAs in image I_S, the *UPPV* of the user U_R
Output: the UPD probabilistic distribution of the *MUA*s in I_S

```
1. for each MUA_j in image I_S do
2.     flag←False;
3.     for each PO_i of the user U_R do
4.         if MUA_j.O=PO_i.O and PO_i.Pr≠0 then
5.             MUA_j.Pr←PO_i.Pr; flag←True;
6.         end if
7.     end for
8.     if flag=False then
9.         perform a distance-based probability propagation of the MUA_j;
10.    end if
11. end for
12. the normalization processing of the |MUA| UPDs is conducted.
```

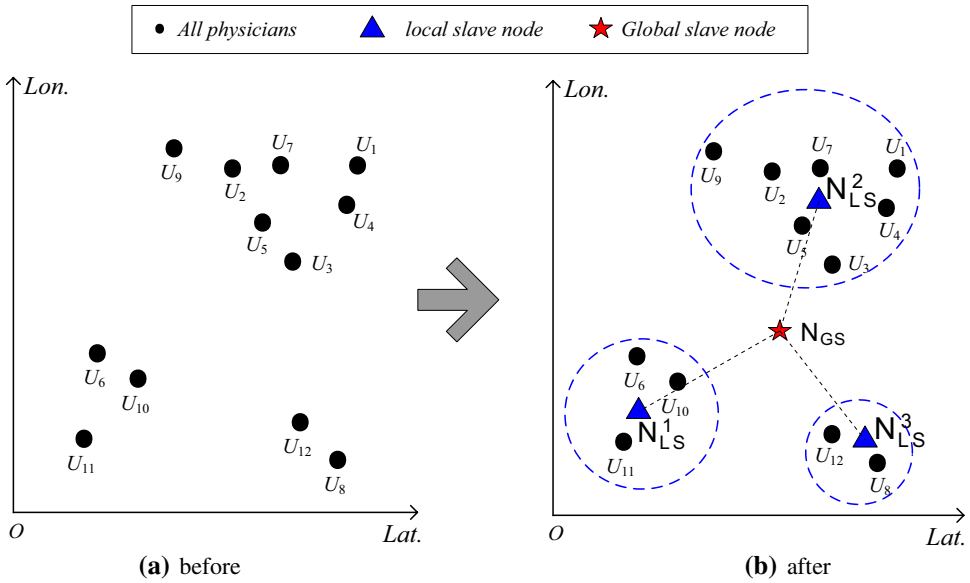

Fig. 8 Learning-based moving trajectory mining

5.2 Optimal IB replica storage scheme

The optimal IB replica storage scheme includes a learning-based slave nodes placement scheme and a UPD-based optimal IB replicas storage scheme.

- *Learning-based slave nodes placement scheme*

As mentioned above, the slave nodes are responsible for the image replicas storage. Since the patients and physicians may not stay at the fixed locations in *MTS*s, the transmission distance between the user and the corresponding slave node may affect the image transmission performance. To minimize the total communication costs, the total distance between all users and their corresponding slave nodes should be minimized. Moreover, as not all of the IB replicas are accessed frequently by users, this motivates us to store the IB frequently accessed replicas separated from those not. This arrangement ensures that frequently accessed IB replicas can be obtained more quickly. Concretely, the IB replicas that are frequently accessed are stored at the slave node which is the nearest to the user, while the IB replicas that are seldom accessed can be stored at the slave one which is relatively far away from the user

Based on the above analysis, in this subsection, we propose a learning-based slave nodes placement scheme. As fast data access is very important to location-based image transmission in *MN*s, the basic idea of this approach is to find an optimal slave nodes placement in the *MN* through mining user movement trajectories.

Theorem 1 *Given m objects: $O_i = (x_i, y_i)$, where $i \in [1, m]$, there exists a centroid object $C = (x_c, y_c)$, the total distance $\sum_{i=1}^{m} (x_i - x_c)^2 + \sum_{i=1}^{m} (y_i - y_c)^2$ is minimal, iif $x_c = \frac{1}{m} \sum_{i=1}^{m} x_i$ and $y_c = \frac{1}{m} \sum_{i=1}^{m} y_i$.*

Proof

$$\sum_{i=1}^{m} (x_i - x_c)^2 + \sum_{i=1}^{m} (y_i - y_c)^2$$
$$= m x_c^2 - 2x_c \sum_{i=1}^{m} x_i + \sum_{i=1}^{m} x_i^2 + m y_c^2 - 2y_c \sum_{i=1}^{m} y_i + \sum_{i=1}^{m} y_i^2$$

Let $\frac{\partial (\sum_{i=1}^{m} (x_i - x_c)^2 + \sum_{i=1}^{m} (y_i - y_c)^2)}{\partial x_c} = 0$, then we have $x_c = \frac{1}{m} \sum_{i=1}^{m} x_i$, $y_c = \frac{1}{m} \sum_{i=1}^{m} y_i$. □

As the users (e.g., patients and physicians) in the *MTS*s are moving constantly, and in most cases, their moving ranges are in relatively fixed areas. To obtain the spatial position of each user, we present a sampling approach to get a representative position of each user.

$$\begin{cases} U_i \cdot pos.lon = \frac{1}{m} \sum_{j=1}^{m} U_i.pos_j.lon \\ U_i \cdot pos.lat = \frac{1}{m} \sum_{j=1}^{m} U_i.pos_j.lat \end{cases} \tag{16}$$

where m is the sampling times.

In Fig. 8a, suppose that there are eleven users (e.g., $U_1 - U_{11}$) with positions obtained by Eq. (16) based on the sampling approach. As shown in Fig. 8b, they are first grouped into three clusters (the dash blue circles) based on

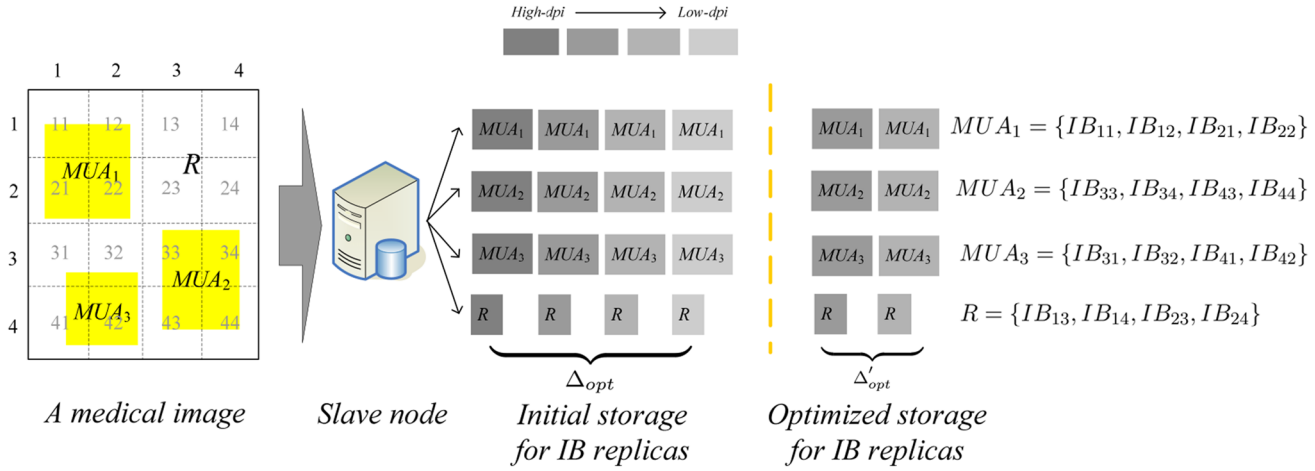

Fig. 9 IB replicas storage

their locations by the DBSCAN clustering algorithm [31]. Based on Theorem 1, the centroid coordinate axis of each cluster (i.e., the coordinate axis of each local slave node) can be derived in the following:

$$\begin{cases} N^j_{\mathrm{LS}}.pos.lon = \frac{1}{|C_j|}\sum_{i=1}^{|C_j|} U_i.pos.lon \\ N^j_{\mathrm{LS}}.pos.lat = \frac{1}{|C_j|}\sum_{i=1}^{|C_j|} U_i.pos.lat \end{cases} \tag{17}$$

where $|C_j|$ means the total number of users in the jth cluster.

For the centroids (N^j_{LS}) in all clusters, the coordinate axes of the global slave node are represented by the following:

$$\begin{cases} N_{\mathrm{GS}}.pos.lon = \frac{1}{|N_{\mathrm{LS}}|}\sum_{i=1}^{|N_{\mathrm{LS}}|} N^i_{\mathrm{LS}}.pos.lon \\ N_{\mathrm{GS}}.pos.lat = \frac{1}{|N_{\mathrm{LS}}|}\sum_{i=1}^{|N_{\mathrm{LS}}|} N^i_{\mathrm{LS}}.pos.lat \end{cases} \tag{18}$$

where $|N_{\mathrm{LS}}|$ means the total number of the local slave nodes.

Summarizing the above description, Algorithm 3 shows our learning-based slave nodes placement algorithm.

Algorithm 3. Learning-based slave nodes placement algorithm

Input: Ω: the image set, t sampling users;
Output: the optimal slave nodes placement;
1. m sampling of the spatial positions of the t users are conducted to obtain their representative positions by Eq.(16);
2. the t sampling users are grouped into k clusters based on their representative positions by the DBSCAN algorithm;
3. **for** each cluster C_j **do**
4. the local slave node position of the cluster C_j is obtained by Eq.(17);
5. **end for**
6. the global slave node position is obtained by Eq.(18);

- *UPD-based optimal IB replicas storage scheme* In this subsection, to facilitate a priority-based image data transmission, we propose a UPD-based optimal IB replicas storage scheme. The basic idea of the storage scheme is that the IBs that are frequently accessed by users are deployed at the nearest local slave node, while other IBs are placed at the global slave one. Specifically, based on the optimal slave nodes placement scheme in Sect. 5.2 and the optimal granularity (Δ_{opt}) in Sect. 5.3, the IB replicas are initially stored in the corresponding nearest local slave node with different pixel resolutions and their corresponding UPDs. For example, there are three MUAs represented by blue rectangles in a medical image in Fig. 9. The IB replicas for the four IFs MUA_1, MUA_2, MUA_3, and R can be stored in the slave nodes with their UPDs information. Algorithm 4 details the initial IB replicas storage processing in N^j_{LS}.

Algorithm 4. ***Initial IB replicas storage*****()**

Input: Ω(j): the images in N^j_{LS}
Output: the initial *IB* replicas placement at the N^j_{LS}
1. **for** each image I_i in Ω(j) **do**
2. its corresponding MUAs are identified;
3. the image is partitioned into several *IB* replicas with different UPDs;
4. the *IB* replicas with different resolutions are stored at the N^j_{LS} based on Δ_{opt};
5. **end for**

In Algorithm 4, the initial number of the IB replicas ($\Delta_{opt} = 4$) is designed for all bandwidth ranging from $E_L = 10$ MB/S to $E_U = 100$ MB/S. In most real-life applications, however, the network bandwidth is relatively stable (i.e., varies in a small range $[E'_L = 80\,\text{MB/S}, E'_U = 90\,\text{MB/S}]$) and the MUAs in the images are identified in advance. This motivate us to investigate an adaptive IB replicas storage scheme based mainly on user access frequencies of the IB replicas. Moreover, the storage efficiency can be significantly improved if the frequently accessed IB replicas can be quickly obtained from the nearest local slave node. Therefore, to further reduce the storage cost of the IB replicas, we propose a batch updating algorithm for the optimal IB replicas storage by mining the users' access logs, which is summarized in Algorithm 5. Specifically, a matrix $M[1 \ldots \Delta_{opt}][1 \ldots |\text{IF}|]$ is initialized to record the user access frequency of each IB replica (line 1). Then, we analyze the access information of each IB by each user (lines 2–9), and sort the user frequencies in a descending order, in which top Δ'_{opt}. IB replicas are obtained as optimal ones (lines 10–11), where $\Delta'_{opt} \leq \Delta_{opt}$. Finally, the optimal Δ'_{opt}. IB replicas are deployed at N^j_{LS}, while other IBs are placed at N_{GS} (lines 12–13). In the batch updating algorithm, we assume that if frequency of new user accesses is larger than a threshold, the batch updating algorithm is performed again.

- *Multi-resolution-based IB replica selection* As mentioned before, since the pixel resolutions of the modern medical imaging systems are very high, this leads to a large data size accordingly. It is non-trivial to transmit such images to the receiver nodes directly, especially in a mobile network environment, in which the network bandwidth is limited and unstable. Therefore, in this subsection, we propose a multi-resolution-based image data replica selection scheme (*MRS*) by comprehensively analyzing the relationship of the image content and network bandwidth.

– *Content and bandwidth-aware optimal pixel resolution selection* As shown in Fig. 10, the basic idea of the MRS method is that for the same medical image, its transmission pixel resolution needs to be adjusted based on the variance of the network bandwidth. Specifically, with high network bandwidth, a high-resolution medical image can be transferred in a reasonable short period of time (θ_T). On the contrary, to get a short response time, a lower resolution version of the same image can be sent to the receiver node with lower network bandwidth.

Although reducing the pixel resolution of the whole image can reduce the transmission overhead, some salient objects

Algorithm 5. ***Batch updating of IB replicas*****()**

Input: the original *IB* replicas storage in N^j_{LS}, *n* sampling users

Output: the updated *IB* replicas placement in N^j_{LS}

1. initialize a matrix: $M[1..\Delta_{opt}][1..|IF|]$ for the *IB* replica IDs; // $M[i][j].freq$=0;
2. **for** each image I_i in $\Omega(j)$ **do**
3. **for** each IB_j in I_i **do**
4. **for** each its corresponding receiver user U_R **do**
5. the optimal ID(i_{opt}) of the IB replica is identified;
6. $M[i_{opt}][j].freq$++;
7. **end for**
8. **end for**
9. **end for**
10. sort the frequency values in the matrix *M* in a descending order;
11. obtain top Δ'_{opt} *IB* replicas as a updated optimal one based on the access frequencies;
12. the optimal Δ'_{opt} *IB* replicas are deployed in N^j_{LS};
13. the rest part of the IB replicas are placed in N_{GS}.

5.3 Adaptive and robust transmission scheme

In this subsection, we propose an adaptive and robust transmission scheme which includes a multi-resolution-based IB replica selection scheme and priority-based IB replica transmission scheme.

(i.e., MUA), however, cannot be clearly examined by the physicians, which may lead to misdiagnosis. Therefore, the resolutions of the MUAs in the image can only be moderately adjusted based on their UPDs, and should be higher than that of the rest part (*R*) of the image. Therefore, the objective of our method is to get a trade-off between the quality

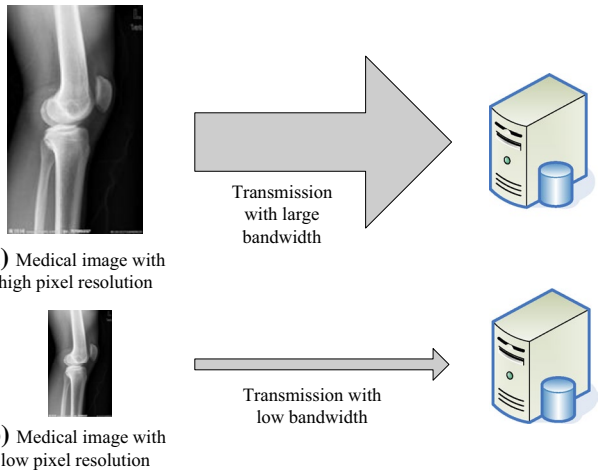

(a) Medical image with high pixel resolution

(b) Medical image with low pixel resolution

Fig. 10 Bandwidth-aware pixel resolution selection

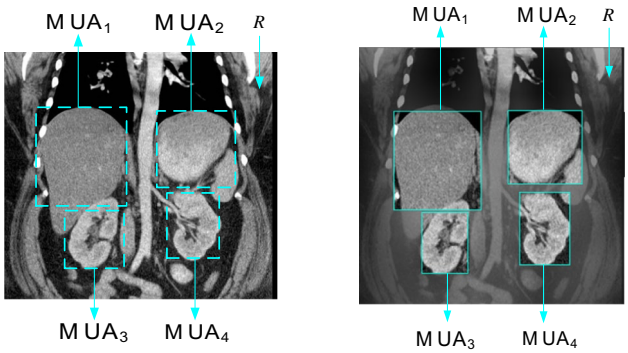

(a) Befor **(b)** After

Fig. 11 Comparison of the pixel resolutions of a same image

of medical images and the transmission time under different resolutions based on the available network bandwidth.

Specifically, let us first denote the average resolution of the image I_S as dpi $\in [D_L, D_U]$, where D_L and D_U mean the lower and upper bounds of dots per inch (*dpi*) of I_S, respectively. For the simplicity of description, we use image fragment (IF) to represent the MUAs and R in the image. Since the IFs are composed of some IBs, the pixel resolutions of the IB replicas can be obtained from that of the IFs. Therefore, the data sizes of the IFs and their corresponding pixel resolutions can be approximately estimated in the following:

$$\begin{aligned}&\sum_{i=1}^{|\mathrm{MUA}|}\left(\mathrm{MUA}_i.S\cdot\mathrm{MUA}_i.dpi^2\right)+R.S\cdot R.dpi^2\\&=\left(\sum_{i=1}^{|\mathrm{MUA}|}\mathrm{MUA}_i.S+R.S\right)\cdot dpi^2\end{aligned}\tag{19}$$

Solving Eq. (19), the average dpi of a whole image can be derived in the following:

$$dpi=\sqrt{\frac{\sum_{i=1}^{|\mathrm{MUA}|}\left(\mathrm{MUA}_i.S\cdot\mathrm{MUA}_i.dpi^2\right)+R.S\cdot R.dpi^2}{\sum_{i=1}^{|\mathrm{MUA}|}\mathrm{MUA}_i.S+R.S}}\tag{20}$$

In addition, the bandwidth of the jth edge is defined as: $E_j \in [E_L, E_U]$, where E_L and E_U are the lower and upper bounds of the bandwidth of the jth edge, respectively. Note that the above bandwidth is a theoretical value, which is larger than the actual one. For the current network bandwidth E_j, we have $E_j \in \left[E_L+\frac{(i-1)\cdot(E_U-E_L)}{\Delta},\ E_L+\frac{i\cdot(E_U-E_L)}{\Delta}\right]$. Since i is an integer, so $i=\left\lceil\frac{(E_j-E_L)\cdot\Delta}{E_U-E_L}+1\right\rceil$, where $\lceil\bullet\rceil$ refers to the integral part of $\bullet$.

Based on an assumption that the average dpi of an image is proportional to the network bandwidth (E_j), the corresponding dpi of I_S under the current network bandwidth (E_j) can be derived as follows:

$$dpi=D_L+\frac{i\cdot(D_u-D_L)}{\Delta}\tag{21}$$

$$dpi=D_L+\left\lceil\frac{(E_j-E_L)\cdot\Delta}{E_U-E_L}+1\right\rceil\cdot\frac{D_U-D_L}{\Delta}\tag{22}$$

where $i \in [1, \Delta]$.

In Eq. (22), a whole image is regarded as an object to be processed. The pixel resolution of the whole image can be adjusted according to the variance of the network bandwidth. This method, however, will lead to the pixel resolution of the MUAs of the image be so low that the physicians cannot clearly examine the image. Therefore, in the preprocessing step, as shown in Fig. 11a, the MUAs in the image are firstly identified by four blue dash rectangles manually, namely MUA_1, MUA_2, MUA_3, and MUA_4. Figure 11b shows that the resolutions of the four MUAs in Fig. 11a and b are moderately changed based on their UPDs, and the resolution of the rest part (R) in Fig. 11b, however, is decreased significantly.

Combining Eqs. (19) and (22), we have

$$\begin{aligned}&\sqrt{\frac{\sum_{i=1}^{|\mathrm{MUA}|}\left(\mathrm{MUA}_i.S\cdot\mathrm{MUA}_i\cdot dpi^2\right)+R.S\cdot R.dpi^2}{\sum_{i=1}^{|\mathrm{MUA}|}\mathrm{MUA}_i.S+R.S}}\\&=D_L+\left\lceil\frac{(E_j-E_L)\cdot\Delta}{E_U-E_L}+1\right\rceil\cdot\frac{D_U-D_L}{\Delta}\end{aligned}\tag{23}$$

Solving Eq. (23), the *dpi* of the rest of the image I_S can be derived as:

$$R.dpi = \sqrt{\frac{\left(\sum_{i=1}^{|\mathrm{MUA}|} \mathrm{MUA}_i.S + R.S\right) \cdot \left(D_L + \left\lceil \frac{(E_j - E_L)\cdot\Delta}{E_U - E_L} + 1 \right\rceil \cdot \frac{D_U - D_L}{\Delta}\right)^2 - \sum_{i=1}^{|\mathrm{MUA}|} (\mathrm{MUA}_i.S \cdot \mathrm{MUA}_i.dpi^2)}{R.S}} \tag{24}$$

Note that, as different MUAs have different UPDs, to ensure the personalized and high pixel resolutions of the MUAs, $\mathrm{MUA}_i.dpi$ can be adjusted based on its UPD (i.e., $\mathrm{MUA}_i.pr$).

As $\mathrm{MUA}_i.dpi$ is proportional to $\mathrm{MUA}_i.pr$, which is represented as:

$$\max_{j\in\lceil 1,|\mathrm{MUA}|\rceil} \{\mathrm{MUA}_j.dpi\} \infty \max_{j\in\lceil 1,|\mathrm{MUA}|\rceil} \{\mathrm{MUA}_j.pr\}. \tag{25}$$

Therefore, the *dpi* of the *i*th MUA can be derived in the following:

$$\mathrm{MUA}_i.dpi = \frac{\max_{j\in[1,|\mathrm{MUA}|]} \{\mathrm{MUA}_j.dpi\}}{\max_{j\in[1,|MUA|]} \{\mathrm{MUA}_j.pr\}} \cdot \mathrm{MUA}_i.pr \tag{26}$$

Combining Eqs. (24) and (26), the *dpi* of the rest part (i.e., *R*) can be derived in the following equation:

$$R.dpi = \sqrt{\frac{\left(\sum_{i=1}^{|\mathrm{MUA}|} \mathrm{MUA}_i.S + R.S\right) \cdot \left(D_L + \left\lceil \frac{(E_j - E_L)\cdot\Delta}{E_U - E_L} + 1 \right\rceil \cdot \frac{D_U - D_L}{\Delta}\right)^2 - \sum_{i=1}^{|\mathrm{MUA}|} \left(\mathrm{MUA}_i.S \left(\frac{\max_{j\in[1,|\mathrm{MUA}|]} \{MUA_j.dpi\}}{\max_{j\in[1,|\mathrm{MUA}|]} \{\mathrm{MUA}_j.pr\}} \cdot \mathrm{MUA}_i.pr\right)\right)}{R.S}}. \tag{27}$$

Note that $\max_{j\in[1,|\mathrm{MUA}|]}\{\mathrm{MUA}_j \cdot dpi\}$ is the original pixel resolution of I_S.

For example, in Fig. 11, given an image, assume that the areas of its corresponding four MUAs are 4 inch^2, 3 inch^2, 2 inch^2, and 1.5 inch^2, respectively. The UPDs of the above four MUAs are 44.8, 18.4, 18.4, and 18.4 %, respectively. The total area of the image is 20 inch^2. The minimal pixel resolution and maximal pixel resolution of the image are: $D_L = 20$ dpi and $D_U = 200$ dpi, and the bandwidth of the mobile network ranges from 10 to 100 MB/S, namely, $E_L = 10$ MB/S and $E_U = 100$ MB/S.

Based on Eq. (27), if the current bandwidth (E_j) is 50 MB/S, then the optimal transmission dpi for the rest part of the image can be derived below:

$$R.dpi = \sqrt{\frac{20 \cdot \left(20\left\lceil \frac{(50-10)\cdot\Delta}{100-10} + 1 \right\rceil \cdot \frac{200-20}{\Delta}\right)^2 - \sum_{i=1}^{4} \left(\mathrm{MUA}_i.S \cdot \left(\frac{200}{0.448} \cdot \mathrm{MUA}_i \cdot pr\right)^2\right)}{20-4-3-2-1.5}}$$

If $\Delta = 10$, then $\mathrm{MUA}_1.dpi = 200$ dpi, $\mathrm{MUA}_2.dpi \approx 82$ dpi, $\mathrm{MUA}_3.dpi \approx 82$ dpi, $\mathrm{MUA}_4.dpi \approx 82$ dpi, and $R.dpi \approx 63$ dpi;

If $\Delta = 20$, then $\mathrm{MUA}_1.dpi = 200$ dpi, $\mathrm{MUA}_2.dpi \approx 82$ dpi, $\mathrm{MUA}_3.dpi \approx 82$ dpi, $\mathrm{MUA}_4.dpi \approx 82$ dpi, and $R.dpi \approx 6$ dpi;...and so on.

– *Optimal Value of* Δ Since the larger Δ is, the larger the storage cost of the IB replicas is. To minimize the above total storage overhead, Δ needs to be minimized. To obtain an optimal Δ, suppose that the image transmission processing can be finished in a transmission deadline (θ_T) set by user, so we have:

$$T_T = T_0 + \frac{Size(I_i)}{BWidth(E_j)} \le \theta_T \tag{28}$$

where

– Size(I_S) is the data size of I_S, represented as: $\mathrm{Size}(I_S) = \left(\sum_{i=1}^{|\mathrm{MUA}|} (\mathrm{MUA}_i.S \cdot \mathrm{MUA}_i.dpi^2) + R.S \cdot R.dpi^2\right) \cdot Bit \cdot CR$, where *Bit* means color bit, and *Bit* can be 8, 16 or 24, *CR* is an image compression ratio, and $CR \in [0,1]$;
– T_0 is the start-up transmission time;
– $BWidth(E_j)$ is a real network bandwidth, represented as $BWidth(E_j) = E_j \cdot TR$, where E_j is a theoretical network bandwidth, TR means a attenuation rate of the bandwidth and $TR \in [0,1]$.

Equation (28) can be rewritten as follows:

$$T_0 + \frac{\left(\sum_{i=1}^{|\mathrm{MUA}|} (\mathrm{MUA}_i.S \cdot \mathrm{MUA}_i.dpi^2) + R.S \cdot R.dpi^2\right) \cdot Bit \cdot CR}{E_i.TR} \le \theta_T \tag{29}$$

$$\sum_{i=1}^{|\mathrm{MUA}|} (\mathrm{MUA}_i.S \cdot \mathrm{MUA}_i.dpi^2) + R.S \cdot R.dpi^2 \le \frac{(\theta_T - T_0)\cdot E_j \cdot TR}{Bit \cdot CR} \tag{30}$$

For the MUAs in the image, Eq. (26) can be derived as follows:

$$\sum_{i=1}^{|\mathrm{MUA}|}(\mathrm{MUA}_i.S\cdot\mathrm{MUA}_i.dpi^2)=\sum_{i=1}^{|\mathrm{MUA}|}\times\left(\mathrm{MUA}_i.S\cdot\left(\frac{\max\limits_{j\in[1,|\mathrm{MUA}|]}\{\mathrm{MUA}_j.dpi\}}{\max\limits_{j\in[1,|\mathrm{MUA}|]}\{\mathrm{MUA}_j.pr\}}\cdot\mathrm{MUA}_i.pr\right)^2\right) \tag{31}$$

For the rest of the image, Eq. (27) is rewritten as follows:

$$R.S\cdot R.dpi^2=\left(\sum_{i=1}^{|\mathrm{MUA}|}\mathrm{MUA}_i.S+R.S\right)\cdot\left(D_L+\left\lceil\frac{(E_j-E_L).\Delta}{E_U-E_L}+1\right\rceil\cdot\frac{D_U-D_L}{\Delta}\right)^2-\sum_{i=1}^{|\mathrm{MUA}|}\left(\mathrm{MUA}_i.S\cdot\left(\frac{\max\limits_{j\in[1,|\mathrm{MUA}|]}\{\mathrm{MUA}_j.dpi\}}{\max\limits_{j\in[1,|\mathrm{MUA}|]}\{\mathrm{MUA}_j.pr\}}\cdot\mathrm{MUA}_i.pr\right)^2\right) \tag{32}$$

Combining Eqs. (30), (31), and (32), we have

$$\left(\sum_{i=1}^{|\mathrm{MUA}|}\mathrm{MUA}_i.S+R.S\right)\cdot\left(D_L+\left\lceil\frac{(E_j-E_L)\cdot\Delta}{E_U-E_L}+1\right\rceil\cdot\frac{D_U-D_L}{\Delta}\right)^2\le\frac{(\theta_T-T_0)\cdot E_j\cdot TR}{Bit\cdot CR} \tag{33}$$

Solving Eq. (33), we have

$$D_L+\left\lceil\frac{(E_j-E_L)\cdot\Delta}{E_U-E_L}+1\right\rceil\cdot\frac{(D_U-D_L)}{\Delta}\le\sqrt{\frac{(\theta_T-T_0)\cdot E_j\cdot TR}{Bit\cdot CR\left(\sum_{i=1}^{|\mathrm{MUA}|}\mathrm{MUA}_i\cdot S+R.S\right)}} \tag{34}$$

Then, Δ can be approximately solved by the following:

$$\Delta\ge\frac{D_U-D_L}{\sqrt{\frac{(\theta_T-T_0)\cdot E_j\cdot TR}{Bit\cdot CR\left(\sum_{i=1}^{|\mathrm{MUA}|}\mathrm{MUA}_i\cdot S+R.S\right)}}-D_L-\frac{(E_j-E_L)\cdot(D_U-D_L)}{E_U-E_L}} \tag{35}$$

To minimize the total storage cost of the image fragment replicas, the value of Δ should be minimized too. Therefore, based on Eq. (35), the optimal value of Δ can be approximately represented below:

$$\Delta_{opt}\approx\left\lceil\frac{D_U-D_L}{\sqrt{\frac{(\theta_T-T_0)\cdot E_j\cdot TR}{Bit\cdot CR\left(\sum_{i=1}^{|MUA|}MUA_i\cdot S+R.S\right)}}-D_L-\frac{(E_j-E_L)\cdot(D_U-D_L)}{E_U-E_L}}\right\rceil \tag{36}$$

For example, given an image, assume that the total area of the image is 20 inch^2, in which the areas of its corresponding three MUAs are 2 inch^2, 4 inch^2, and 5 inch^2, respectively. The minimal pixel resolution and maximal pixel resolution of an image are: $D_L = 20$ dpi and $D_U = 200$ dpi. In addition, the bandwidth of the mobile network ranges from 10 to 100 MB/S, namely, $E_L = 10$ MB/S and $E_U = 100$ MB/S. $T_0 = 0.1$ s, $\theta_T = 0.6$ s, $TR = 0.1$, $CR = 0.05$, and $Bit = 16$.

Based on Eq. (36), if the current network bandwidth(E_j) is 50 MB/S, then the optimal value of Δ is 7.

– *Optimal ID of IB replica* In the above, we have obtained an optimal granularity (Δ_{opt}). Next, we study how to choose an optimal ID of each IB replica among its Δ_{opt} replicas.

For the rest of the image, as the lower and upper bounds of the *dpi* (i.e., D_L and D_U), the ID number (i) of the image fragment (R) replica and are met in the following equation:

$$D_L+\frac{D_U-D_L}{\Delta_{opt}}\cdot i=R.dpi \tag{37}$$

where Δ_{opt} is equal to that of in Eq. (36).

As i is an integer, solving Eq. (37), we have:

$$i=\left\lceil\frac{(R.dpi-D_L)\cdot\Delta_{opt}}{D_U-D_L}\right\rceil \tag{38}$$

If $\left|D_L+\frac{D_U-D_L}{\Delta_{\mathrm{opt}}}\cdot\left\lceil\frac{(R.dpi-D_L)\cdot\Delta_{opt}}{D_U-D_L}\right\rceil-R.dpi\right|\le\left|D_L+\frac{D_U-D_L}{\Delta_{opt}}\cdot\left(\left\lceil\frac{(R.dpi-D_L)\cdot\Delta_{opt}}{D_U-D_L}\right\rceil+1\right)-R.dpi\right|$ then the optimal ID of the IB replica for the rest part is derived in the following:

$$i_{opt}=\left\lceil\frac{(R.dpi-D_L)\cdot\Delta_{opt}}{D_U-D_L}\right\rceil \tag{39}$$

Otherwise, the optimal ID of the IB replica for the rest part is as follows:

$$i_{opt}=\left\lceil\frac{(R.dpi-D_L)\cdot\Delta_{opt}}{D_U-D_L}\right\rceil+1 \tag{40}$$

Similarly, for the MUAs in the image, we have

$$D_L+\frac{D_U-D_L}{\Delta_{opt}}\cdot i=\mathrm{MUA}_i.dpi \tag{41}$$

Therefore, the optimal ID of the IB replica for the ith MUA is derived in the following:

$$i = \left\lceil \frac{(\mathrm{MUA}_i.dpi - D_L) \cdot \Delta_{opt}}{D_U - D_L} \right\rceil \tag{42}$$

If $\left| D_L + \frac{D_U - D_L}{\Delta_{opt}} \cdot \left\lceil \frac{(\mathrm{MUA}_i.dpi - D_L) \cdot \Delta_{opt}}{D_U - D_L} \right\rceil - \mathrm{MUA}_i.dpi \right| \leq \left| D_L + \frac{D_U - D_L}{\Delta_{opt}} \cdot \left(\left\lceil \frac{(\mathrm{MUA}_i.dpi - D_L) \cdot \Delta_{opt}}{D_U - D_L} \right\rceil + 1 \right) - \mathrm{MUA}_i.dpi \right|$ then the optimal ID of the IB replica for the MUA_i is derived in the following:

$$i_{opt} = \left\lceil \frac{(\mathrm{MUA}_i.dpi - D_L) \cdot \Delta_{opt}}{D_U - D_L} \right\rceil \tag{43}$$

Otherwise, the optimal ID of the IB replica for the MUA_i is as follows:

$$i_{opt} = \left\lceil \frac{(\mathrm{MUA}_i.dpi - D_L) \cdot \Delta_{opt}}{D_U - D_L} \right\rceil + 1 \tag{44}$$

– *Priority-Based IB replicas transmission scheme* Generally speaking, in most of the state-of-the-art image data transmission schemes, an image is transferred as a whole object, in which the transmission priority of each IB is equal. Thus, it is possible that the important MUAs in the image be displayed later than the rest of the image (i.e., non-MUA). Moreover, for the medical images with high pixel resolutions, this transmission method, however, will lead to more failures in the transmission process. Once transmission failure occurs, the image needs to be re-transferred, which results in a higher transmission overhead. To overcome this technical bottleneck, we propose a priority-based image block data robust transmission scheme called *PIBT* to support successive transmission of large image data. The transmission priority (*TP*) of each IB is based on its UPD, which is defined in the following.

$$IB.TP = \begin{cases} \mathrm{UPD}(\mathrm{MUA}_i, U_R) & \mathrm{IB} \in \mathrm{MUA}_i \\ 0, & \text{Otherwise} \end{cases} \tag{45}$$

where $\mathrm{UPD}(\mathrm{MUA}_i, U_R)$ can be derived by Algorithm 2 and the IB belongs to the MUA_i. As different IBs have its corresponding *TP*s, the IBs can be transmitted based on their corresponding *TP*s in a descending order, which not only ensures the robustness of data transmission, but also guarantees that the important information can be transmitted first.

6 The UMIT algorithm

With the support of the above enabling techniques, a medical image can be efficiently transferred in the *MTS*. Algorithm 6 summarizes the detailed steps of our proposed *UMIT* processing. First of all, a user U_R sends an image transmission request (i.e., the ID number of I_S) to the master node N_M (line 1), then the *UPPV* of U_R is obtained from the PUS (lines 2–6) and the IBs in I_S are identified (line 7). After that, the network bandwidth, user's professional preference vector, etc., are collected and analyzed to obtain an optimal pixel resolutions and the UPDs of the IB replicas (i.e., MUAs), respectively (lines 8–12). Finally, the transmission request is sent to the global slave node to identify if the corresponding IB replicas are at the nearest neighbor (*NN*) local slave node. If so, the IB replicas at the NN N_{LS} are sent to the receiver node based on their transmission priorities in a descending order (line 14); otherwise, they are transmitted from the N_{GS} (line 16).

Algorithm 6. ***UMIT***(I_S, U_R)

Input: I_S: a transmission image and some parameters, a user U_R
Output: the image transferred
1. an image transmission request is submitted from N_R by U_R;
2. **if** U_R is from *PUS* **then**
3. obtain his *UPPV* by user matching;
4. **else**
5. perform the user preference propagation processing to obtain his *UPPV*;
6. **end if**
7. **if** the MUAs have not been identified in I_S **then** identify the MUAs in this image;
8. **for** each IB_i in I_S **do** *// at the master node*
9. it corresponding optimal pixel resolution and th transmission priority of its replica are obtained by the OMR scheme based on the network bandwidth and the *UPD*;
10. its transmission priority is defined in Eq.(45);
11. **end for**
12. the transmission request is sent to the global slave node;
13. **if** the corresponding *IB* replicas are in the NN N_{LS} **then**
14. they are transmitted from N_{LS} based on their transmission priorities in a descending order;
15. **else**
16. they are transmitted from N_{GS} based on their transmission priorities in a descending order;
17. **end if**

7 Experimental evaluation

To verify the efficiency and reliability of the proposed *UMIT* method, we conduct simulation experiments to demonstrate the transmission performance of our scheme.

7.1 Experiment setup

The image receiver client is run on the Android platform [34] and implemented in the Java language. Each node has a 2.7 GHz Xeon processor, 2 GB memory, and 1 TB hard disk. The nodes in the local area network are connected via 1 Gbps network links. The number of nodes in our system varies from 10 to 100. The maximum data communication rate is 100 Mbps in the mobile network. In the slave nodes, the IB replicas with different pixel resolutions are stored in a file system and some key information is recorded in a MySQL [35] database.

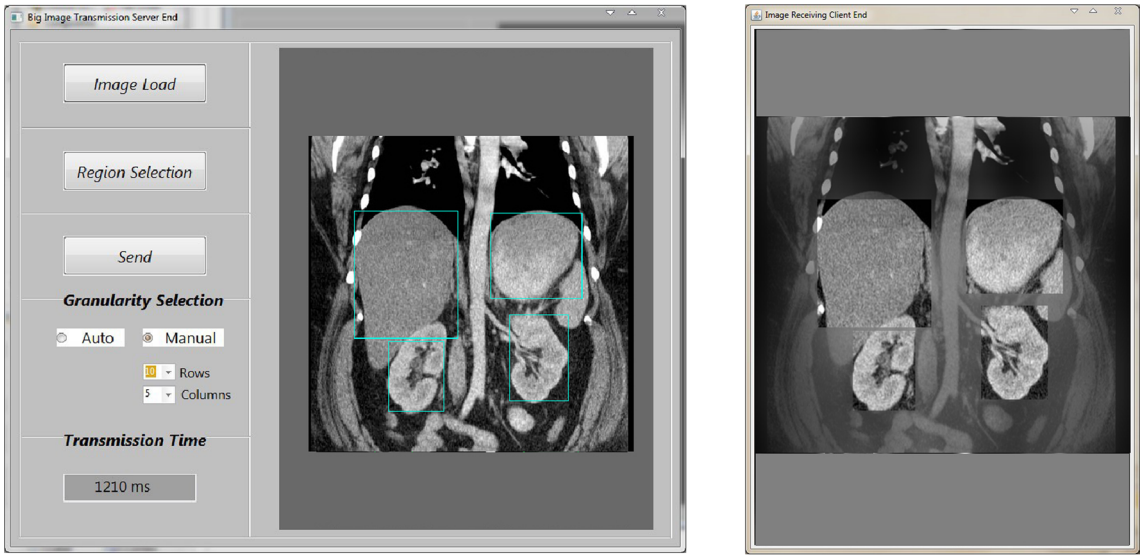

(a) An backend interface **(b)** An client end interface

Fig. 12 User-adaptive medical image transmission system

Fig. 13 Effect of the image size

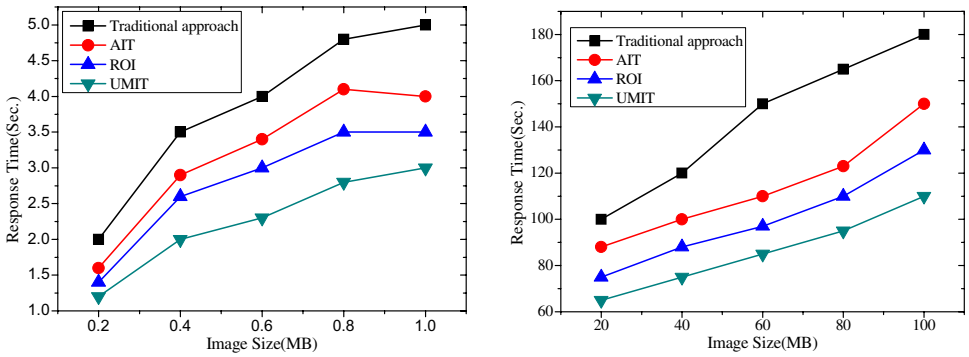

(a) Real dataset **(b)** Synthetic dataset

Fig. 14 Effect of the network bandwidth

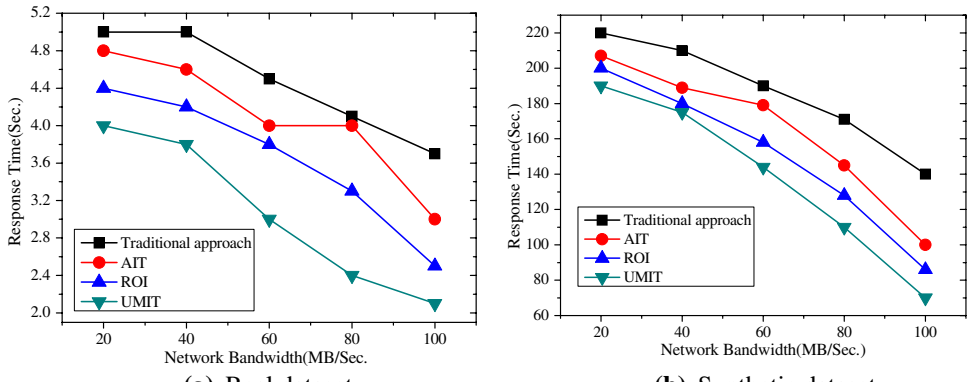

(a) Real dataset **(b)** Synthetic dataset

Fig. 15 Effect of Δ

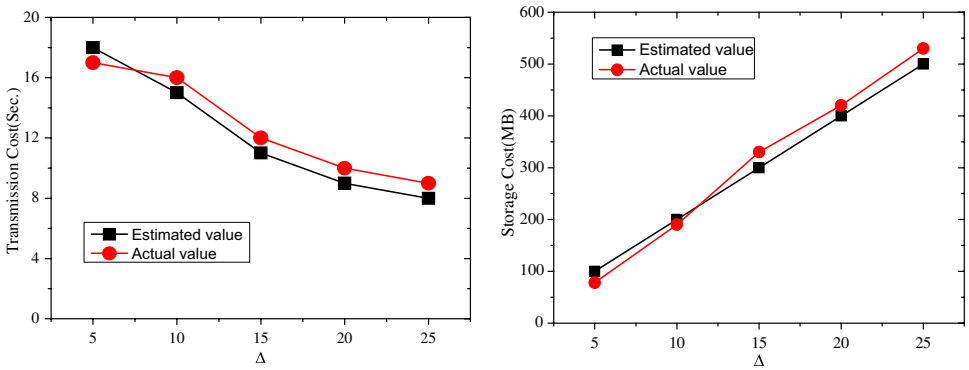

(a) Δ *vs.* transmission cost **(b)** Δ *vs.* storage cost

- *Datasets* The medical image data sets for our experiment are obtained from two ways: (1) Real data set: 100,000 medical images are downloaded from the Medical image archive [33], in which the image data size ranges from 0.2 to 1 MB; (2) Synthetic data set: To evaluate the effect of data size on the image transmission performances, we have synthesized five groups of the medical image data, in which the data size of each image is 1, 5, 10, 50, and 100 MB, respectively.
- *Competitors* In the following experiments, we compared our proposed method (*UMIT*) with the three competitor methods. Method 1 uses the traditional transmission method (i.e., transmitting the whole medical image without partition). Method 2 adopts the adaptive image transmission (*AIT*) [11]. Method 3 uses a new Region of Interest (*ROI*)-based approach to improve wireless electronic healthcare service quality [3].

7.2 A prototype transmission system

We have implemented a prototype transmission system for medical images, as shown in Fig. 12. Figure 12a shows an example of the back-end interface of the offline medical image processing. The four MUAs in this figure have been identified by four green rectangles. Figure 12b demonstrates the receiver (e.g., hepatologist) client interface, in which the IBs in the five IFs (i.e., the four MUAs represented by the four green-line rectangles and the rest part *R*) have been reconstructed and displayed. Moreover, the pixel resolutions of the four MUAs are higher than that of the rest part, and the resolution of the MUA region of '*liver*' is the highest among the four MUAs when the image receiver is a hepatologist.

7.3 Effect of image size

In the first experiment, we study the effect of the image size on the performance of the *UMIT* processing using the above two kinds of image data. For each method, we measured the average time required to transmit an image. In Fig. 13a and b, when the bandwidth (e.g., 100 MB/S) is relatively stable, the total transmission time using the *UMIT* is superior to that of other three. Meanwhile, with the increase of the image data size, the performance gap of the four approaches becomes enlarged when the image size is increasing. This is because compared with the *UMIT* approach, for the traditional one, its corresponding data size of the images to be transmitted is increasing so rapidly that the images cannot be sent to the destination nodes quickly. Our proposed hybrid pixel resolution approach can effectively reduce the transmitted image data, especially for a large image.

7.4 Effect of network bandwidth

Next, we investigate the effect of network bandwidth on the performance of the *UMIT* processing using the two kinds of images mentioned. Figure 14 shows when the image data sizes (i.e., 0.5 MB for real data and 50 MB for the synthetic data) are fixed, the total response time using the *UMIT* is better than that of the three ones. Meanwhile, with the condition that the bandwidth is increasing, the response time decreases gradually and the performance gap becomes larger especially for the large synthetic image data. This is because in the *UMIT*, compared with the original image data size, it has to be reduced based on the network bandwidth, the image content, and so on, resulting in a significant decrease in the transmission cost.

7.5 Effect of Δ

In this experiment, we proceed to test the effect of Δ on the transmission and storage costs, respectively. In Fig. 15a, when Δ is from 5 to 25, the transmission cost is gradually decreasingly; while in Fig. 15b, the storage cost increases with the increase of Δ. This is because when Δ is small, the data size of each IB replica is relatively larger. Thus, the transmission cost dominates. Similarly, the total number of the IB replicas is increasing when Δ becomes larger, which

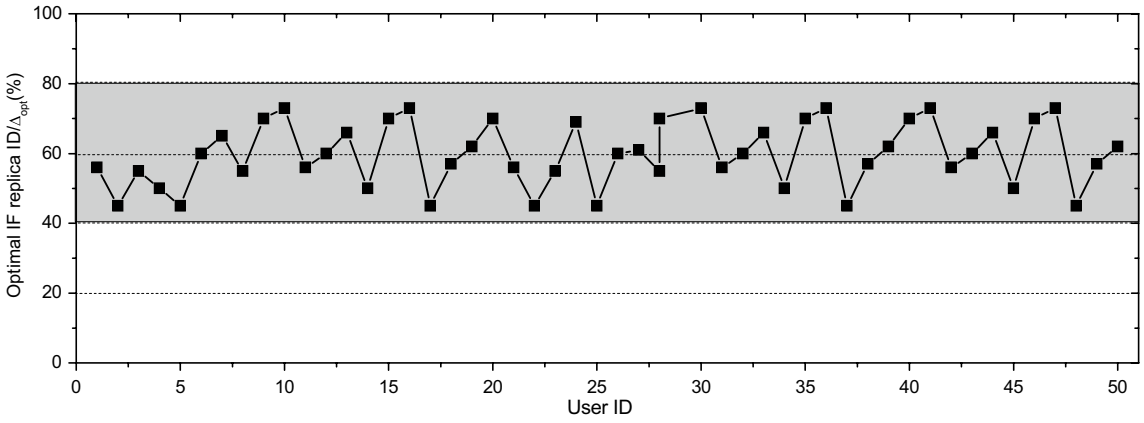

Fig. 16 Distribution of the optimal IB replica ID

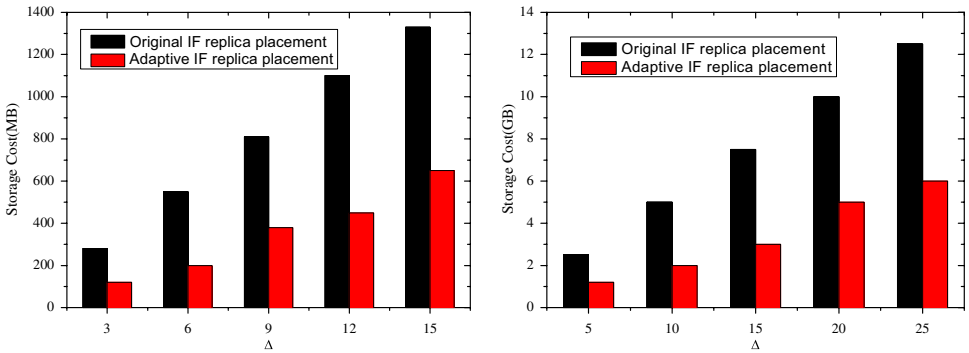

Fig. 17 Effect of IB replica placement scheme

(a) Real dataset **(b)** Synthetic dataset

leads to the larger storage cost of the IB replicas. Therefore, obtaining a trade-off between transmission cost and storage cost with an optimal Δ is critically important to the *UMIT* processing.

7.6 Effect of IB replica placement scheme

In this experiment, we study the effect of the two IB replica placement schemes using the two data sets of image sizes 100 and 500 MB, respectively.

First of all, we conducted 50 *UMIT*s processing, in which the 50 images to be transmitted are randomly selected from the data set. Figure 16 illustrates that the ratio of the optimal IB replica ID to Δ_{opt} ranges from 40 to 80 %, which means only a part of the IB replicas has been accessed.

Next, we test the effect of IB replica placement scheme on the storage costs. Method 1 uses the original IB replica placement scheme and Method 2 adopts the adaptive one. In Fig. 17, when the Δ is from 3(5) to 15(25), the storage costs are gradually increasing, while the storage cost by Method 1 is larger than that of Method 2. It is obvious that the adaptive IB replica placement scheme can significantly reduce the storage cost, since the optimal IB replicas are part of the whole ones, which is verified in Fig. 16.

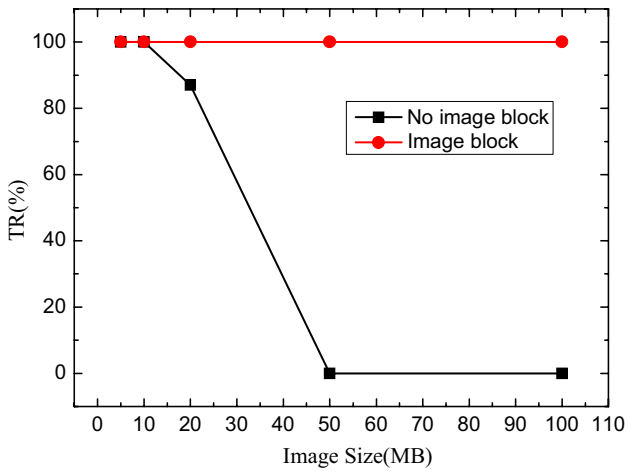

Fig. 18 Image size vs. transmission robustness

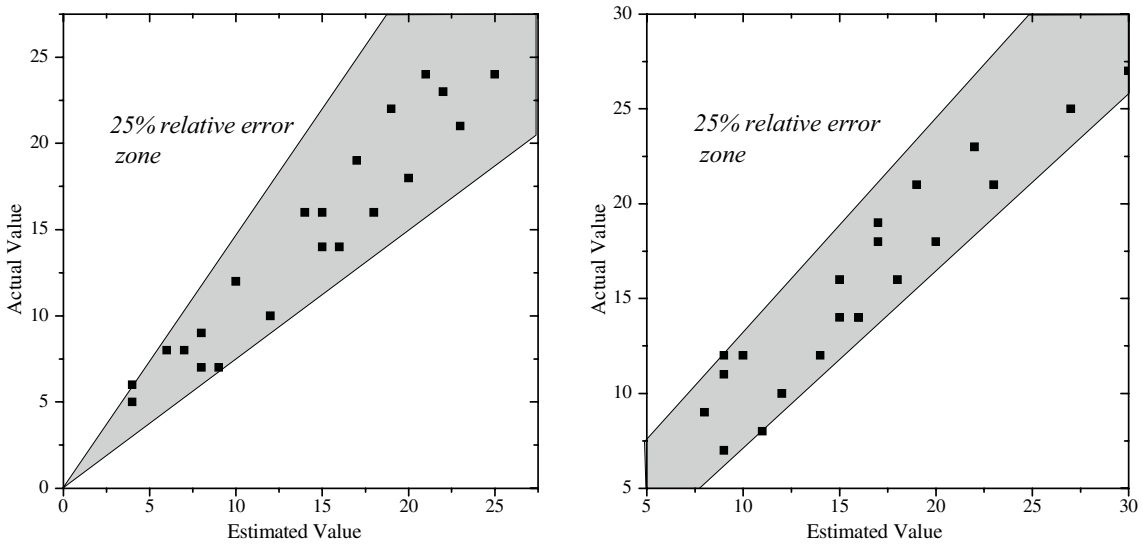

(a) Real dataset **(b)** Synthetic dataset

Fig. 19 Evaluation of optimal Δ

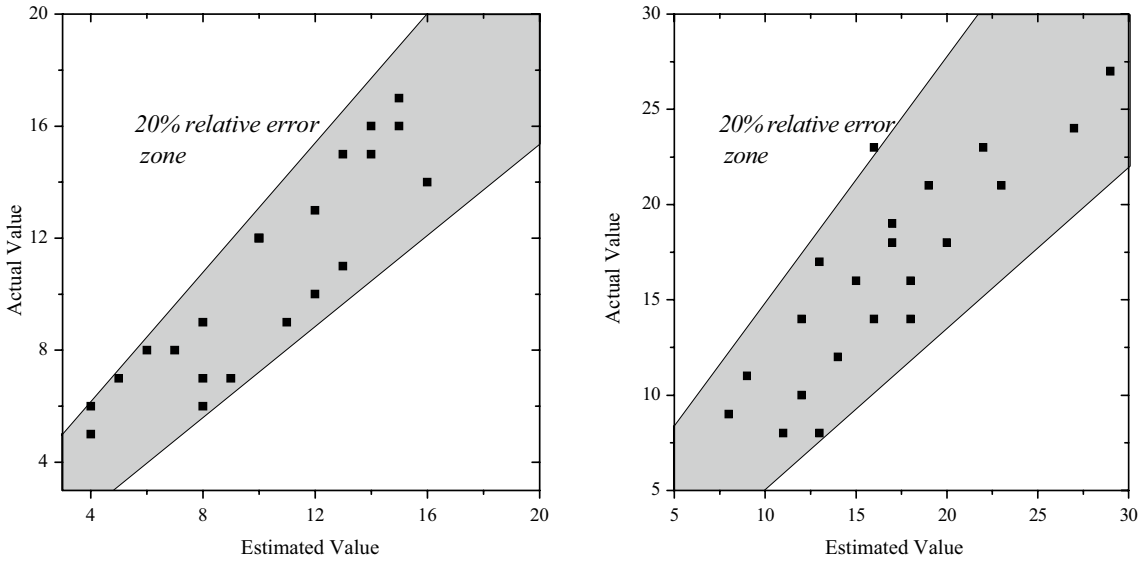

(a) Real dataset **(b)** Synthetic dataset

Fig. 20 Evaluation of optimal replica ID

7.7 Robustness comparison

In this experiment, to evaluate the effect of image size on the transmission robustness, we then used the synthetic image data set, in which the images have been divided into five groups in terms of the data size 5, 10, 20, 50, and 100 MB, respectively. Two transmission schemes are tested: (1) Image blocking method and (2) No image blocking one. The transmission reliability (*TR*) can be defined in the following:

$$TR = \frac{Number\ of\ sucessful\ data\ transmissions}{Total\ number\ of\ data\ transmissions} \quad (46)$$

As shown in Fig. 18, with the increase of data size, the successful data transmission ratio is 100 % using the image fragmentation technique. For the data transmission without adopting our *UMIT* method, when the transmission data size is less than 10 MB, the successful transmission ratio is 100 %. However, if the data size is 20 MB, the average *TR* is

decreased to 87 %; and if the data size is larger than 50 MB, the average *TR* is zero, as it is hard to transmit such a large image successfully. Based on the experimental result, to guarantee a high successful data transmission ratio, it is only possible to transfer a large image through the image blocking method under limited network bandwidth.

7.8 Evaluation of optimal Δ

This experiment evaluates the optimal Δ presented in Sect. 5.3 for the *UMIT* processing. For the above two image data sets, we have performed the 20 *UMIT*s processing, in which the image is randomly selected from the three image sets, respectively. Figure 19 shows the actual and estimated optimal replica ID of each transmission (i.e., the horizontal and vertical coordinates of a plotted point, respectively). Ideally, all points would fall on the diagonal of the act-est space (i.e., actual and estimated values are equal). The shaded area covers transmissions for which our technique yields up to 25 percent relative error, where the relative error (*RE*) can be defined as follows:

$$RE = \frac{|actual\ value - estimated\ value|}{actual\ value} \tag{47}$$

It is interesting to notice that for the synthetic image data, in most cases, the optimal Δ is larger than that of the two real image data. The is because for a large image data, in most cases, the smaller the segmentation granularity is, the higher the probability that the suitable (optimal) IB replicas are obtained. To minimize the image transmission time, especially for the large image data, its corresponding number of the IB replicas should be larger than that of others.

7.9 Evaluation of optimal replica ID

Finally, we evaluate the optimal replica ID presented in Sect. 5.3. Suppose the optimal Δ is fixed, we have conducted 20 *UMIT*s processing, in which the network bandwidth, the selection of the MUAs, and their corresponding UPDs, etc., are randomly generated in this experiment. Figure 20 shows, for the two image data sets, the actual and estimated optimal replica ID of each transmission. Ideally, all points would fall on the diagonal area. The shaded area covers transmissions for which our technique yields up to 20 percent relative error. For the synthetic image data, the optimal replica ID is larger than other two. The reason is similar to that explained in Sect. 7.8.

8 Conclusions and future work

In this paper, we have presented a professionally user-adaptive medical image transmission scheme (*UMIT*) in *MTS*, which specifically caters for user preference and needs, together with different bandwidth availabilities in *MN*. Three enabling techniques, namely, *UPD derivation of MUAs, optimal IB replica storage scheme*, and *adaptive and robust transmission scheme*, are proposed to reduce the data communication overhead. Our experiments demonstrate that the proposed *UMIT* method is efficient and effective for large medical image transmission in minimizing the network communication cost and maximizing the parallelism of I/O and CPU.

In our future work, we will focus on the following:

1. Facing the challenges of transmission intensive applications, to further improve the whole throughput of the transmissions, we shall investigate a pipeline-based distributed transmission optimization technology to further speed up the transmission efficiency in the mobile network environments;
2. Last but not the least, besides image transmission processing, we shall investigate a progressive transmission scheme for complex media types, such as 3D objects, animation, video, etc.

Acknowledgments The authors would like to thank the editors and anonymous reviewers for their helpful comments. This work is partially supported by the Program of the National Natural Science Foundation of China under Grant Nos. 61272188, 61540064, 61379075; the Ministry of Education of Humanities and Social Sciences Project under Grant No. 14YJCZH235; the "Qianjiang Talent" Project of Zhejiang Province under Grant No. QJD1402017; the National Science & Technology Pillar Program under Grant No. 2014BAK14B01; and the Program of Natural Science Foundation for Distinguished Young Scholars of Zhejiang Province.

References

1. Qureshi, A., Shoeb, A., Guttag, J.: Building a high-quality mobile telemedicine system using network striping over dissimilar wireless wide area networks. In: Proc. of Annual Int'l Conf. on IEEE Engineering in Medicine and Biology Society, vol. 4, pp. 3942–3945 (2005)
2. Maani, R., Camorlinga, S., Arnason, N.: A parallel method to improve medical image transmission. J. Digit Imaging **25**(1), 101–109 (2012)
3. Wang, W., Zhao, M., Wang, H., Hua, K.: Exploring region of interest (ROI) to support quality of service in unreliable wireless electronic healthcare communications. Int. J. Healthc. Inf. Syst. Inf. **7**(4), 1–12 (2012)
4. Charles, J.T., Larry, L.P.: Image transfer: an end-to-end design. In: ACM SIGCOMM Int'l Conference on Data Communication, pp. 258–268 (1992)
5. John, M.D., Georey, M.D., Song, X.Y.: Fast lossy internet image transmission. In: ACM Int'l Conference on Multimedia (1995)
6. Raman, S., Balakrishnan, H., Srinivasan, M.: An image transport protocol for the Internet. In: Int'l Conference on Network Protocol, pp. 209–219 (2000)
7. Allcocka, B., Bestera, J., Bresnahan, J., et al.: Data management and transfer in high-performance computational grid environments. Parallel Comput. **28**(5), 749–771 (2002)

8. Lin, T., Hao, P.: Compound image compression for real-time computer screen image transmission. IEEE Trans. Image Process. **14**(8), 993–1005 (2005)
9. Ruiz, V.G., Fernández, J.J., García, I.: Image compression for progressive transmission. In: In the Nineteenth IASTED Int'l Conference on Applied Informatics: Advances in Computer Applications, Innsbruck, pp. 519–524 (2001)
10. Gao, D.H., Liu, D.H., Feng, Y.Q., et al.: A robust image transmission scheme for wireless channels based on compressive sensing. In: Advanced Intelligent Computing Theories and Applications. With Aspects of Artificial Intelligence. Lecture Notes in Computer Science, vol. 6216, pp. 334–341 (2010)
11. Chang, R.C., Shih, T.K., Hsu, H.H.: A strategic decomposition for adaptive image transmission. J. Inf. Sci. Eng. **24**(3), 691–707 (2008)
12. Chang, C.C., Shine, F.C., Chen, T.S.: A new scheme of progressive image transmission based on bit-plane method. In: Asia-Pacific Conference on Communications and Fourth Optoelectronics and Communications Conference, vol. 2, pp. 892–895 (1999)
13. Chang, C.C., Shih, T.K., Lin, I.C.: An efficient progressive image transmission method based on guessing by neighbors. Vis. Comput. Int. J. Comput. Graph. **18**, 341–353 (2002)
14. Chang, C.C., Wu, M.N.: A color image progressive transmission method by common bit map block truncation coding approach. In: Int'l Conference on Communication Technology, vol. 2, pp. 1774–1778 (2003)
15. Kim, J.H., Song, W.J.: Pyramid-structured progressive image transmission using quantization error delivery in transform domains. IEE Vis. Image Signal Process. **143**, 132–136 (1996)
16. Tzou, K.H.: Progressive image transmission: a review and comparison of techniques. Opt. Eng. **26**, 581–589 (1987)
17. Boluk, P.S., Baydere, S., Emre Harmanci, A.: Robust image transmission over wireless sensor networks. J. Mob. Netw. Appl. **16**(2), 149–170 (2011)
18. Aziz, S.M., Pham, D.M.: Energy efficient image transmission in wireless multimedia sensor networks. IEEE Commun. Lett. **17**(6), 1084–1087 (2013)
19. Sun, Y., Xiong, Z.-X.: Progressive image transmission over space-time coded OFDM-based MIMO systems with adaptive modulation. IEEE Trans. Mob. Comput. **5**(8), 1016–1028 (2006)
20. Victor, S., Abugharbieh, R., Nasiopoulos, P.: 3-D scalable medical image compression with optimized volume of interest coding. IEEE Trans. Med. Imaging **29**(10), 1808–1820 (2010)
21. Arslan, S.S., Cosman, P.C., Milstein, L.B.: Generalized unequal error protection LT Codes for progressive data transmission. IEEE Trans. Image Process. **21**(8), 3586–3597 (2012)
22. Zhuang, Y., Jiang, N., Wu, Z., Li, Q., et al.: Efficient and robust large medical image retrieval in mobile cloud computing environment. Inf. Sci. (INS) **263**, 60–86 (2014)
23. Hoppe, H.: Progressive meshes. In: Proceedings of SIGGRAPH'96, pp 77–108 (1996)
24. Teler, E., Lischinski, D.: Streaming of complex 3d scenes for remote walkthroughs. In: Computer Graphics Forum (Eurographics 2001 Conference Proceedings), vol. 20, no. 3, pp. 17–25 (2001)
25. Rusinkiewicz, S., Levoy, M.: Streaming qsplat: a viewer for networked visualization of large, dense models. In: ACM Interactive 3D 2001 Conference Proceedings, pp. 63–69 (2001)
26. Gu, X., Gortler, S.J., Hoppe, H.: Geometry images. ACM Trans. Graph. **21**(3), 355–361 (2002)
27. Bischoff, S., Kobbelt, L.: Towards robust broadcasting of geometric data. Comput. Graph. **26**, 665–675 (2002)
28. Lamberti, F., Sanna, A.: A streaming-based solution for remote visualization of 3D graphics on mobile devices. IEEE Trans. Vis. Comput. Graph. **13**(2), 247–260 (2007)
29. Cheng, W., Ooi, W.T., Mondet, S., Grigoras, R., Morin, G.: An analytical model for progressive mesh streaming. In: In the 15th ACM International Multimedia Conference, September 24–29, pp 737–746(2007)
30. Kumar, S., Mishra, M.K.: 3D object transmission over internet using 2D image streaming technology. Int. J. Adv. Res. Electron. Commun. Eng. (IJARECE), **2**(4), 410–414 (2013)
31. Ester, M., Kriegel, H.-P., Sander, J., Xu, X.W.: A density-based algorithm for discovering clusters in large spatial databases with noise. In: Proc. of the Second Int'l Conference on Knowledge Discovery and Data Mining (KDD-96), pp. 226–231 (1996)
32. Gal, V., Kerre, E., Tikk, D.: Organ detection in medical images with discriminately trained deformable part model. In: Prof. of 2013 IEEE 9th Int'l Conf. on Computational Cybernetics (ICCC), pp. 153–157 (2013)
33. The medical image dataset. http://www.ece.ncsu.edu/imaging/Archives/ImageDataBase/Medical/index.html (2009)
34. The Android platform http://www.google.com/android (2010)
35. MySQL http://www.mysql.com/ (2010)